Numerical Investigation of the Influence of Constructive Aspects on the Structural Behaviour of Masonry Cross Vaults

Numerical investigation of the influence of constructive aspects on the structural behaviour of masonry cross vaults

M. Alforno[a]*, F. Venuti[a], A. Monaco[a] and C. Calderini[b]

[a]*Department of Architecture and Design, Politecnico di Torino, Torino, Italy*

[b]*Department of Civil, Chemical and Environmental Engineering, University of Genoa, Genova, Italy*

*e-mail: marco.alforno@polito.it

Abstract

In this paper the structural performance of masonry cross vaults is investigated with regard to the most common differential settlements occurring in historical constructions. Numerical parametric models are developed for vaults with different brick patterns and lateral constraints, in the presence/absence of infill. In particular, radial, diagonal and pitched brick patterns are taken into account and opening, shear and vertical settlements are analyzed. Moreover, the behaviour of laterally unconfined vaults is compared with the response of vaults restrained with rigid perimeter walls or with lateral masonry arches. The analyses highlight the strengths and weaknesses of each configuration, providing a scientific validation to some speculations found in historical technical literature on the most widespread use of some brick patterns. The outcomes of this research provide a deep knowledge of masonry vaults behaviour in view of more effective interventions on historical buildings, supplying the practitioners with a crack-pattern chart useful for better interpreting the damage pattern in historical vaults with different brick courses.

Keywords

masonry vaults; masonry apparatus; brick pattern; numerical models; structural analysis

1. Introduction

Cross masonry vaults are common structural elements in historical buildings, often employed because of the great flexibility they offer from an architectural point of view. They were built with various materials and construction techniques, but when blocks were adopted (i.e., stone or bricks), specific rules had to be followed to create the masonry apparatus. Great attention to this topic was given in the European technical literature published in the 19th century (e.g. Lassaulx 1829; Breymann 1849; Curioni 1870; Choisy 1883). This careful description of brick laying techniques, often accompanied by technical drawings, highlights the relevance given to this topic by ancient builders.

Various authors (Breymann 1849; Chevalley 1924; Donghi 1906; Formenti 1893; Gelati 1907; Levi 1932) describe different possible brick configurations for various vaults typologies and offer some considerations regarding when and why it is more suitable to choose a pattern instead of another. Often, the choice of a certain brick pattern was related to the constructive phases of the vaults (for a review, see Wendland 2007, Alforno et al. 2020b, Boni et al. 2021) and in particular with the possibility to build without formwork (Wendland, 2007). In other cases, as demonstrated by Di Pasquale (1983) in its fundamental study on the dome of Santa Maria del Fiore in Florence, the choice of a certain brick pattern was related to the search for a better structural response.

According to literature, in European cross vaults the direction of the courses varies from radial (i.e., principal joints parallel to the ring arch of the caps, Figure 1a) to diagonal (i.e., courses on diagonally tilted planes perpendicular to the groins, Figure 1b) to vertical (or pitched, Figure 1c).

In the case of radial courses (Figure 1a), a formwork is required, just like in the case of a barrel vault with the same pattern or in the case of an arch (not stable until the key stone is positioned). When this pattern is used, good interlocking should be provided at the intersection of the caps, in order to strengthen the groins and prevent cracking along these lines. The diagonal pattern (Figure 1b) is a rather common masonry apparatus in European cross vaults. In this pattern, every new brick course is self-supporting with an arch-like curvature. However, wood centering is required in order to support the diagonal arches during construction, whereas the rest of the surfaces could be built arranging self-supporting courses to be spanned conveniently between the centering arches. Cross vaults can also be built entirely without any formwork or centering, in a procedure that is based on pitched bricks technique (Lancaster 2015) and consists of the intersection of four barrel vaults with transversal, almost vertical, arched courses that are built simultaneously starting from the four surrounding walls (Figure 1c). The arched courses are inclined and the intersection at the groins can occur, as in the case of the radial pattern, by interlocking subsequent courses along the groin lines. This way of building vaults developed in Egypt and in the Middle East and was used in mud brick architecture from at least the third millennium BCE (van Beek 1987). This brick pattern was not quite common in the European tradition, apart from the region of Extremadura, Spain (Florencio Ger y Lobez, 1869) and was almost exclusively confined to the Middle East (Wendland, 2007).

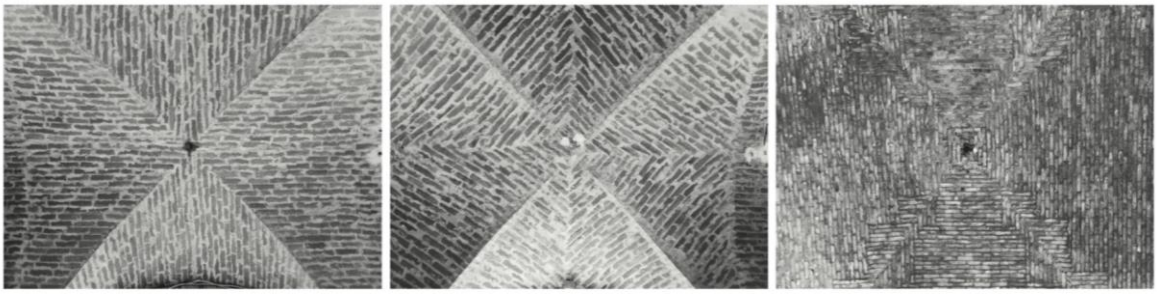

Figure 1: possible brick pattern in real cross vaults: radial (a), diagonal (b), pitched (c). Portico of the Palazzata in Vicoforte (a, b) and Palazzo della Pilotta in Parma (c)

As stated in several of the aforementioned treatises, brick pattern played a key role, both in terms of construction feasibility and expected structural performance. However, this speculation was grounded on empirical observations of vaults behavior. In recent structural engineering literature, despite the structural behavior of vaults has been extensively investigated (e.g., Lourénço, De Borst, and Rots 1997; Huerta 2001; Milani et al. 2006; Milani et al. 2016; Rossi et. al 2016; Tralli et al. 2014), the role of the masonry apparatus is addressed far less often, with a few exceptions (Barbieri et al. 2004, Calderini and Lagomarsino 2004, Romano and Grande 2008, Baratta and Corbi 2012, Foraboschi 2014, Foti et al. 2018, Alforno et al. 2020b, Boni et al. 2021). Baratta and Corbi (2012) stressed that the brick pattern plays a role of paramount importance in the definition of the equilibrium of the vaults because it is useful to individuate the path stresses within the structure. As an example, these authors compared the qualitative response of two pavilion vaults of equal geometry but with different masonry apparatus (bed joints parallel to the vault perimeter, in one case, and bed joint orthogonal to the perimeter in the other case). So doing, they were able to demonstrate that a different distribution of the horizontal thrust occurs along the perimeter, the preferred equilibrium path being that of having compression normal to the bed joints. Other authors stressed the role of the brick pattern also in masonry domes. In particular, Foraboschi (2014) compared the behavior of the monumental dome of Santa Maria del Fiore in Florence by Brunelleschi and the Vasari's dome in Basilica della Madonna dell'Umiltà in Pistoia, finding that the Vasari's dome, similar to Brunelleschi's dome but built with a different brick apparatus, underwent cracks at the ribs (instead of in the webs) since its construction phase and therefore the dome needed to be immediately reinforced after its completion.

A very limited number of scientific studies have been devoted to systematically investigating the effects of the brick pattern on the behaviour of masonry vaults by adopting numerical approaches. In the past, few studies proposed a macro-modelling approach. Among them, Barbieri et al. (2004) adopted the Finite Element Method to investigate the behaviour of a barrel vault under self-weight, with five different orientations of bed joints. The model of the vault was built using shell elements and giving orthotropic linear elastic material properties to masonry. The orientation of the bed joints was reproduced by properly rotating the shell element local axes. Different results in stiffness were put into evidence; in particular, the authors showed that the vault with the most widespread pattern (90° between the bed joints and the head arch plane) exhibited the lowest

stiffness. Calderini and Lagomarsino (2004) used the homogenization theory for specifically taking into account the peculiarities of the brick pattern. Their model was used for developing non linear analyses on an ideal vault subjected to both self-weight and asymmetric concentrated force; different stress distributions and failure loads were found depending on the brick pattern. The influence of the masonry apparatus was also investigated by Romano and Grande (2008) on barrel vaults, adopting both macro- and micro-modelling approaches and analyzing the case of both vertical and horizontal settlements. Also in these cases, non linear analyses were performed for showing that different brick patterns bring different stiffness and ultimate load at failure.

The most recent works adopt a micro-modelling approach, which is more suitable to properly account for the actual brick laying. Foti et al. (2018) and Boni et al. (2021) modelled vaults using Discrete Element Method (DEM), adopting a macro-block discretization of the vault surface. Specifically, Foti et al. studied the behaviour of cross vaults undergoing settlements of the supports, while Boni et al. modelled barrel, cross and pavilion vaults subject to self-weight and concentrated loads. Both studies demonstrated the influence of the masonry apparatus on the vault collapse mechanism. A more geometrically-refined model was proposed by Alforno et al. (2020b), who adopted a Finite Element Method (FEM) simplified micro-modelling approach, where the real brick dimensions are taken into account in the surface discretization. The authors analysed the behaviour of barrel and cross vaults under self-weight with different brick patterns, providing a scientific validation to some speculations found in historical technical literature.

In general, it can be noted that block-based models represent a powerful modelling strategy for the behaviour of masonry at the scale of the heterogeneity of the assemblage of ashlars and mortar or even dry joints. In this frame, contact-based approaches are widely adopted, basically assuming that several rigid or deformable blocks interact each other through contact areas ruled by frictional or cohesive laws. DEM models are typically based on contact penalty formulations and explicit integration and they are mainly used for applications where blocks are considered undeformable or linear elastic. DEM models usually result in quite fast analyses with contained computational demand if compared with other numerical methods, and therefore they also allow full-scale applications. However, in general, they are not appropriate for the simulation of masonry crushing which can be essential in some failure mechanisms. To this aim, FEM modeling can be a more powerful and suitable strategy for taking into account the mechanical nonlinearities of blocks in tension and compression. FEM modelling is more versatile to achieve different analysis scopes taking advantage of the opportunity of properly detailing the mechanical features of the masonry assemblage.

The present work aims at carrying on the investigation started by Alforno et al. (2020b) on the effects of masonry apparatus on the static behavior of masonry vaults through a micro-modelling FEM approach developed with Abaqus 2019 (Abaqus 2019). Specifically, this study focuses on cross vaults undergoing differential settlements of the supports. Moreover, the effects of boundary conditions and infill are also explored on the vault with radial pattern, which is one of the most widespread in the European tradition. The

results of this study aim to deepen the knowledge of masonry vaults behaviour in view of more effective interventions on historical buildings.

The paper develops in the following Sections: first, the adopted numerical approach is described in Section 2; Section 3 is devoted to the description of the ideal cross masonry vaults adopted as case study and of the parametric analysis; results of the numerical simulations, in terms of load-displacement curves, deformed shapes and contour plots of vertical displacements, are commented on in Section 4; finally, in the concluding section, a crack pattern chart is provided to help identifying the reasons of incipient collapse mechanisms in existing vaults.

2. Description of the numerical approach

The adopted method of analysis consists in a simplified micro-modelling finite element approach, which follows a quite standard procedure widely described in the technical literature (among others Lourenço et al. 1995). This type of model is based on the accurate reproduction of the real 3D geometry of the vault with its brick pattern. The geometry of the structural model is obtained as the assemblage of a set of elastic blocks connected with zero-thickness non-linear interfaces. The tensile strength of interfaces is null, while their normal contact in compression is assumed almost rigid by the introduction of a high value of normal stiffness so that:

$$\sigma_c = k_n \cdot \delta_n \quad (1)$$

where δ_n is the displacement occurring after the normal contact between two nodes of the model. Eq. (1) represents the well-known "penalty method", which admits that a small amount of penetration between nodes in contact can take place, but sufficiently high values of k_n ensure that the penetration is negligible. The penalty method is computationally more efficient than the absolute rigid normal behavior because it facilitates the convergence of the analysis. The choice of an almost rigid contact in compression allows for the concentration of the overall elastic deformability of the system within the resisting blocks.

The tangential behaviour of interfaces is implemented through a purely frictional model, in which the contribution of cohesion is neglected:

$$\tau_{fr} = -\sigma_c \cdot \mu \quad (2)$$

In Eq. (2) τ_{fr} is the tangential stress, σ_c the compressive stress and μ the static friction coefficient. Under these assumptions, only few mechanical parameters are needed for modeling masonry vaults: the material density ρ, elastic modulus E and Poisson's coefficient ν of masonry and the interface friction coefficient μ.

When studying historical masonries, usually both tensile strength and cohesion of mortar joints are neglected because of the degradation of the mechanical properties of the material due to aging. Moreover, several studies in the literature have shown that tensile strength and cohesion of joints plays a limited role in the failure mode and crack patterns of vaulted masonry structures (D'Altri et al. 2019). As already shown by the Authors in some previous research (Alforno et al. 2020a,b), this approach can be used for both the cases

of vaults made up of bricks and mortar layers and vaults constructed with stones and dry joints. In the first case, the mortar thickness is included within the dimension of the masonry blocks and the mechanical parameters adopted for both blocks and interfaces have to be capable of taking into account for the role of the mortar joints. Conversely, in the second case, the geometry and the mechanical properties of the masonry blocks coincide with those of the stones while the interface behavior has to be simply modeled as stone-to-stone contact.

From a mechanical point of view, the goal of the model is to perform static analyses for simulating the response of a cross vault under different imposed displacements corresponding to opening, shear and vertical differential settlements. The load conditions will be described in detail in the following sections. However, when contact problems are modeled, several convergence issues may arise. Therefore, dynamic implicit analysis is conducted for investigating the structural behaviour under quasi-static regime in order to control and stabilize the numerical convergence of the solution (Abaqus 2019). Finally, geometrical nonlinearities are taken into account.

3. Description of the case study

3.1. Geometry and mechanical parameters

The adopted case study is an ideal cross masonry vault generated by the intersection of two semi-circular barrel vaults. It has a square base, with a net span of approximately 3.1 m and rise of 1.175 m. This geometry mimics in full scale the one of the physical model described in Rossi et al. (2016) and numerically simulated in Milani et al. (2016), Gaetani et al. (2020) and Alforno et al. (2020a). The discretization of the vault's geometry is performed with blocks of the size of typical bricks (6 x 12 x 24 cm), except for the blocks along the diagonal arches, which were modified in order to simplify the definition of interfaces in the FEM environment (Figure 2).

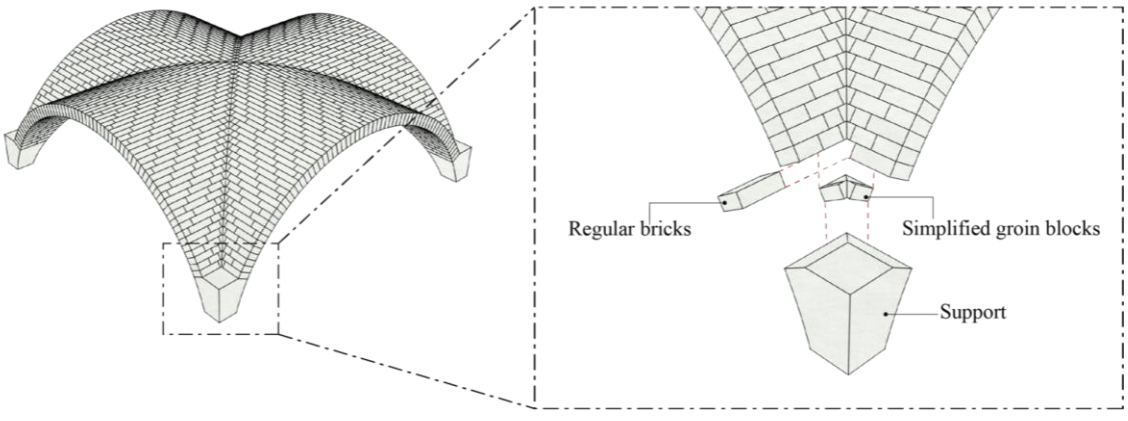

Figure 2: Discretization of the vault's geometry

Mechanical properties of blocks and interfaces are summarized in Table 1. The adopted values are those suggested in Rossi et al. (2016). The value of the normal stiffness in compression k_n has been calibrated by the Authors to assure quasi-rigid contact. For limiting high computational demand, the calibration procedure was

carried out on a circular arch that coincides with the vault's head arch. The analysis consists of an imposed horizontal displacement of one support (Figure 3a). The displacement at collapse u_c has been determined for increasing value of k_n in the range $5 \cdot 10^7$–$5 \cdot 10^{17}$ N/m^3. Figure 3b plots the load-displacement curves obtained for $k_n = 5 \cdot 10^9$ N/m^3 and Figure 3c plots the displacement at collapse u_c versus k_n. From the second plot, it can be noted that the ultimate displacement remains almost constant for values of k_n above $5 \cdot 10^9$ N/m^3; therefore, this was assumed as the minimum value to have almost rigid contacts.

Table 1: mechanical properties of blocks and interfaces

Blocks			**Interfaces**	
ρ [kg/m^3]	E [MPa]	ν [-]	μ [-]	k_n [N/m^3]
1800	1200	0.2	0.5	$5 \cdot 10^9$

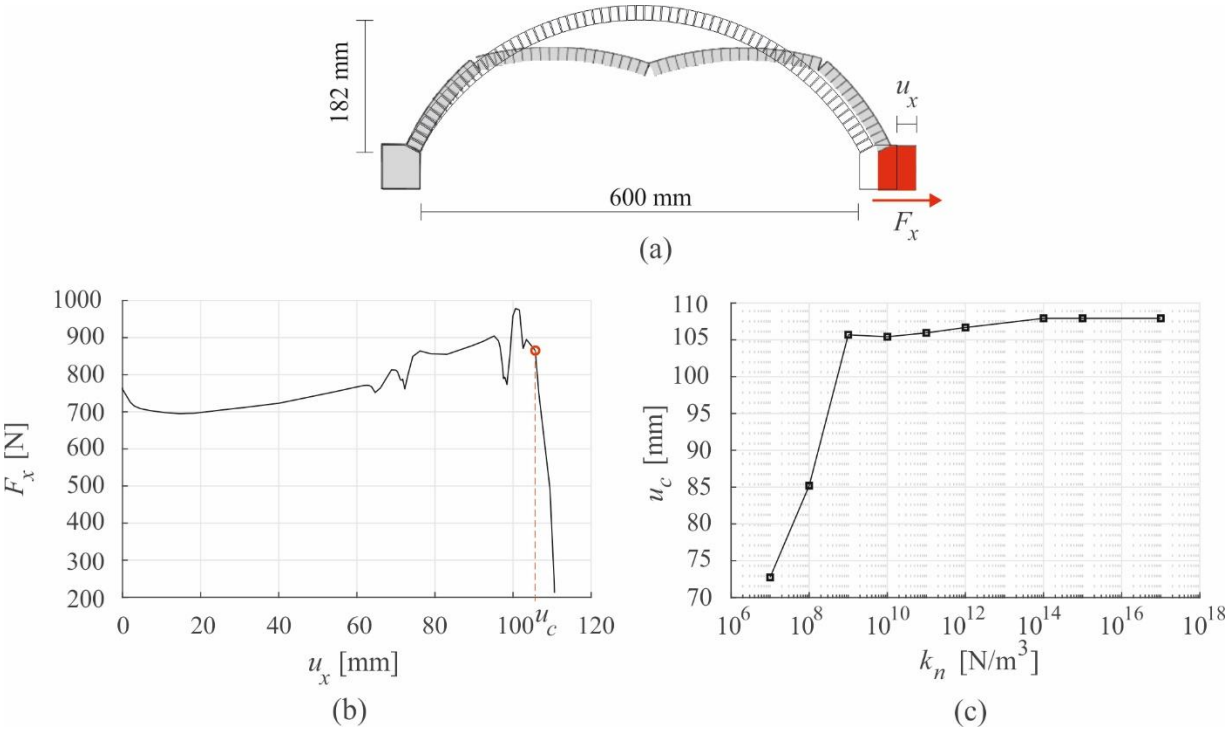

Figure 3: scheme of the arch with imposed settlement u_x (a), load-displacement curve for $k_n = 5 \cdot 10^9$ N/m^3 (b) and displacement u_c at collapse versus k_n (c).

3.2. Actions

The vault is subject to its self-weight and to settlements of the abutments. Three kinds of displacements are applied: a horizontal displacement u_x of two abutments in x direction, resulting in an Opening (O) mechanism (Figure 4a); a horizontal displacement u_y of two abutments in y direction, resulting in a Shear (S) mechanism (Figure 4b); a Vertical (V) settlement u_z of two abutments in z direction (Figure 4c).

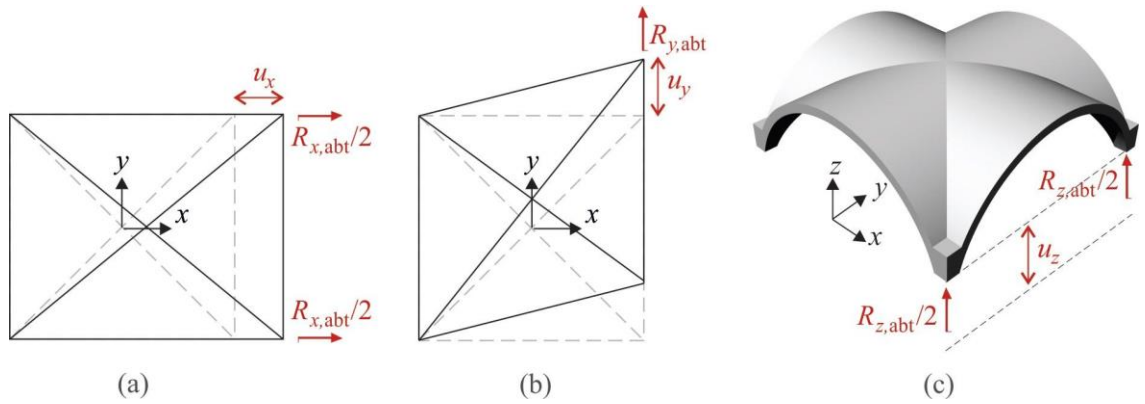

Figure 4: scheme of the imposed displacements and measured reaction forces at the abutments: opening (a), shear (b) and vertical (c) settlement.

3.3. Parametric analyses

The following constructive aspects are taken into account in the subsequent parametric analyses: brick pattern; vault boundary conditions; presence of infill.

The three patterns represented in Figure 5 have been considered: radial (bed joints perpendicular to head arches), diagonal (bed joints perpendicular to groins) and pitched pattern (slightly inclined courses parallel to head arches).

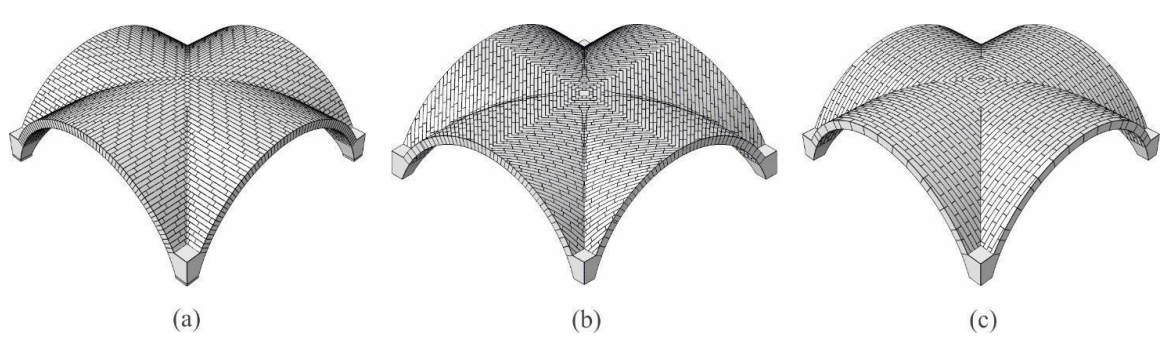

Figure 5: Radial (a), diagonal (b) and pitched (c) masonry pattern.

Concerning the boundary conditions, different lateral restraints of the head arches have been considered (Figure 6). In the first one (Figure 6a), the vault is Not Confined (NC). In particular, previous studies conducted by the Authors (Alforno at al. 2020b) have demonstrated that pitched and diagonal vaults are not stable without confinement and therefore this condition is applied on the radial vault only. In the second case, the out-of-plane displacements of the head arches of the vault are Rigidly Constrained (RC) (Figure 6b). This is the case of vaults included within stiff walls, as often occurs in historic palaces. This condition is modelled by introducing on the perimeter of the vault stiff lateral planes, whose external surfaces are restrained against out-of-plane displacements and whose internal surfaces are connected to the head arches of the vault by zero-thickness interfaces with the same mechanical properties used for defining the block-to-block contacts. This means that normal compressive forces can arise between the lateral walls and the vault, while no tension forces can develop, resulting in the possibility of detachment between the head arches of the vault and lateral walls.

Moreover, shear forces along the planes of the boundary structures can be generated, depending on the normal forces, according to a Mohr-Coulomb criterion. The third case is introduced to reproduce the shear behavior of porches or lateral naves of churches undergoing seismic actions. In this case the vaults are constrained by a wall on one side only, while on the other sides it is confined by lateral Deformable Arches (DA). Such arches have about twice the vault thickness (27 cm) and 50 cm depth (Figure 6c) and are again connected to the head arches of the vault by zero-thickness interfaces with the same mechanical properties used for defining the block-to-block contacts.

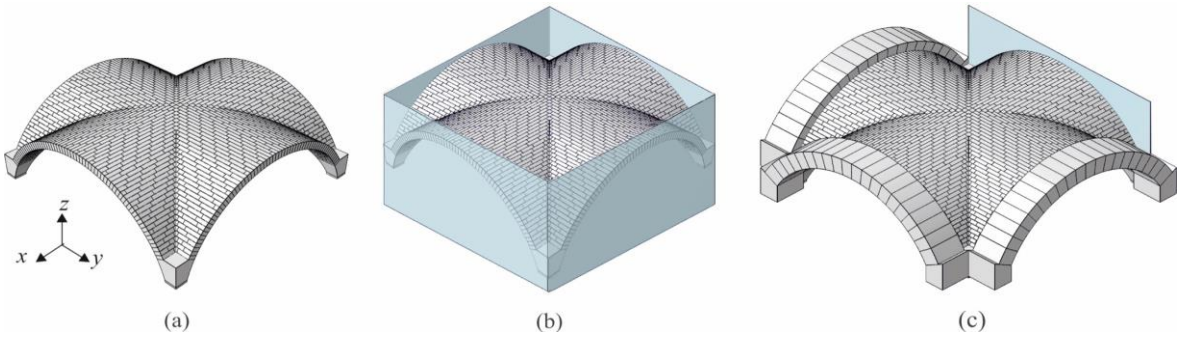

Figure 6: no confinement (NC) (a), rigid lateral confinement (RC) (b) and boundary deformable arches (DA) (c)

Finally, the influence of infill is investigated. For the sake of simplicity, only NC radial cross vault was considered for this study. This a purely theoretical choice, since in real structures the infill actually needs to be confined by lateral walls. The infill is modelled as a set of nodal forces proportional to the mass of a volume 10 cm higher than the vault key and 900 kg/m^3 heavy. Such nodal forces are applied on the extrados of the vault and are aligned to the *z*-axis (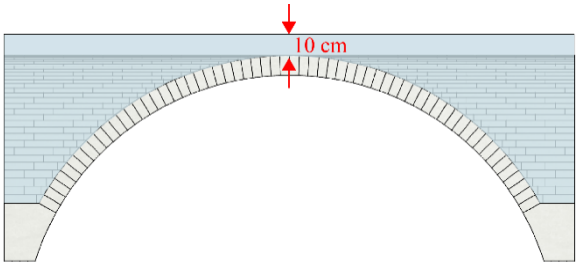

). Even if it seems to play a relevant role in the structural response of vaults (Gelfi 2002), lateral thrusts due to earth filling were not considered in the analysis.

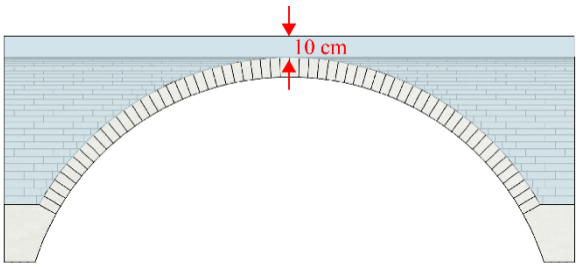

Figure 7: volume of infill (in blue)

Table 2 summarizes the set of the fifteen performed parametric analyses.

Table 2: Summary of the parametric analyses set up

Brick Pattern			Boundary condition			Infill		Load condition		
Radial	Diagonal	Pitched	NC	RC	DA	No	Yes	O	S	V
■			■			■		■		
■			■			■			■	
■			■			■				■
■				■		■		■		
■				■		■				■
■					■	■			■	
■			■				■	■		
■			■				■		■	
■			■				■			■
	■			■		■		■		
	■			■		■				■
	■				■	■			■	
		■		■		■		■		
		■		■		■				■
		■			■	■			■	

4. Results

4.1. Static behaviour under self-weight

The behaviour of the vaults is firstly analyzed under self-weight. The infill is not considered here. In Figures Figure 8-Figure 10, the amplified deformed shapes of the vaults with the three different patterns are shown. It can be observed that both the pitched and the diagonal vaults are not stable without confinement (Figure 8a and Figure 9a) (Alforno at al. 2020b). For all the considered patterns, rigid boundaries allow for lower vertical displacements of the entire vault surface.

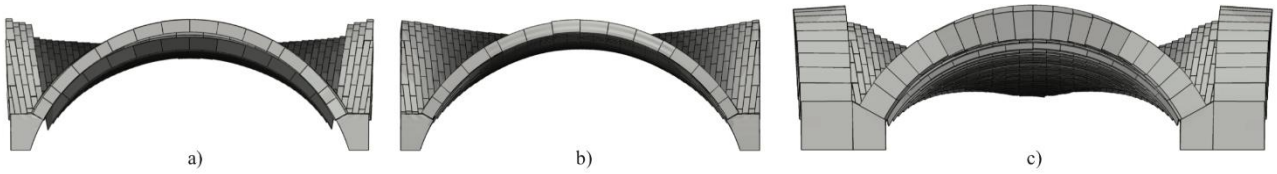

Figure 8: Pitched cross vault without confinement (a), with rigid confinement (b) and with deformable arches (c) under self-weight (amplification factor =100).

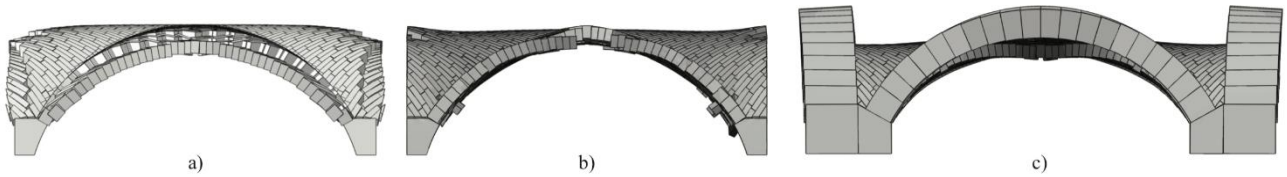

Figure 9: Diagonal cross vault without confinement (a), with rigid confinement (b) and with deformable arches (c) under self-weight (amplification factor =100).

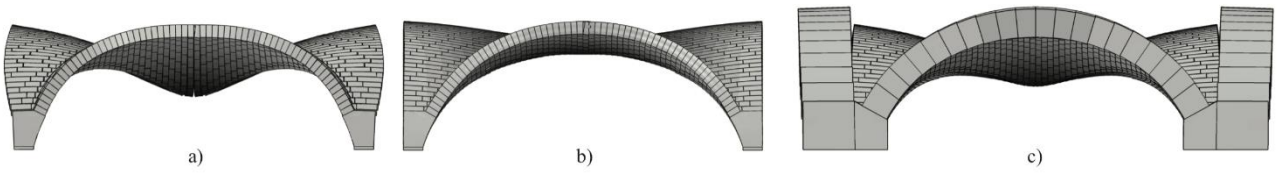

Figure 10: Radial cross vault without confinement (a), with rigid confinement (b) and with deformable arches (c) under self-weight (amplification factor =100).

In Table 3 and Table 4, the horizontal thrusts of the vaults at the abutments on one side of the vault ($R_{x0,\mathrm{abt}}$), as well as the resultants of the horizontal thrust on the confining structures (either rigid planes or deformable arches) ($R_{x0,\mathrm{con}}$) and the overall resultants of the thrusts ($R_{x0,\mathrm{tot}}$), are reported. The vertical displacement of crown u_{z0} is also given. In general, it can be observed that the rigidly confined vaults (RC cases) have larger overall thrusts on the confining structures and smaller vertical displacements of crowns. In the RC cases, the ratio $\eta = R_{x0,\mathrm{con}} / R_{x0,\mathrm{abt}}$ between the thrust against the rigid boundary and at the vault abutments increases when passing from radial (η = 2.08) to diagonal (η = 3.33) to pitched (η = 4.23): this is expected due the fact that both diagonal courses and pitched courses lay against the rigid boundary. In the DA case, the ratio η has the same value as in the RC case for the radial vault. Conversely, for diagonal and pitched vaults, the thrust exerted by diagonal and pitched courses cannot be appropriately contrasted by the deformable arch, therefore η is lower than unit (η = 0.81 and η = 0.68 respectively).

Table 3: horizontal thrusts due to self-weight R_{x0} and vertical displacement of crown u_{z0} for vault confined with rigid boundaries (RC).

Pattern	$R_{x0,\mathrm{abt}}$ [N]	$R_{x0,\mathrm{con}}$ [N]	$R_{x0,\mathrm{tot}}$ [N]	u_{z0} [cm]	η
Radial	4727	9843	14570	0.471	2.08
Diagonal	2902	9679	12581	0.310	3.33
Pitched	3232	13678	16909	0.425	4.23

Table 4: horizontal thrusts due to self-weight R_{x0} and vertical displacement of crown u_{z0} for vault confined with deformable arches (DA).

Pattern	$R_{x0,\mathrm{abt}}$ [N]	$R_{x0,\mathrm{con}}$ [N]	$R_{x0,\mathrm{tot}}$ [N]	u_{z0} [cm]	η
Radial	3375	6828	10203	0.733	2.02
Diagonal	6064	4936	11000	0.520	0.81
Pitched	6623	4493	11116	0.863	0.68

4.2. Effects of brick pattern in confined vaults for the different load conditions

4.2.1. Opening settlement (O)

This settlement is studied with the rigid lateral restraint condition (RC) only. The test is performed by moving two abutments in the *x*-direction, as well as the RC connected to those abutments. The other RC and two abutments are kept fixed. Note that no connection is provided between the RCs, therefore immediate separation is allowed.

The deformed shapes in Figure 11 allow observing quite different collapse mechanisms depending on the masonry pattern. While the radial vault displays a more global mechanism, with formation of hinges in the normal direction with respect to the imposed settlement, both diagonal and pitched vaults display local failure

that mainly involve the cap near the moving abutments. This is especially true for the pitched pattern, where the collapse mechanism does not affect the global stability of the entire structure but involves a few series of ring arches connected to the moving abutments in the *y-z* plane, while the rest of the vault maintains its bearing capacity thanks to the confining effect due to the lateral rigid boundaries. Such confinement prevents the normal detachment between adjacent brick courses in the remaining three caps of the vault and, thanks to the friction, the sliding of the head arches along the supporting structures.

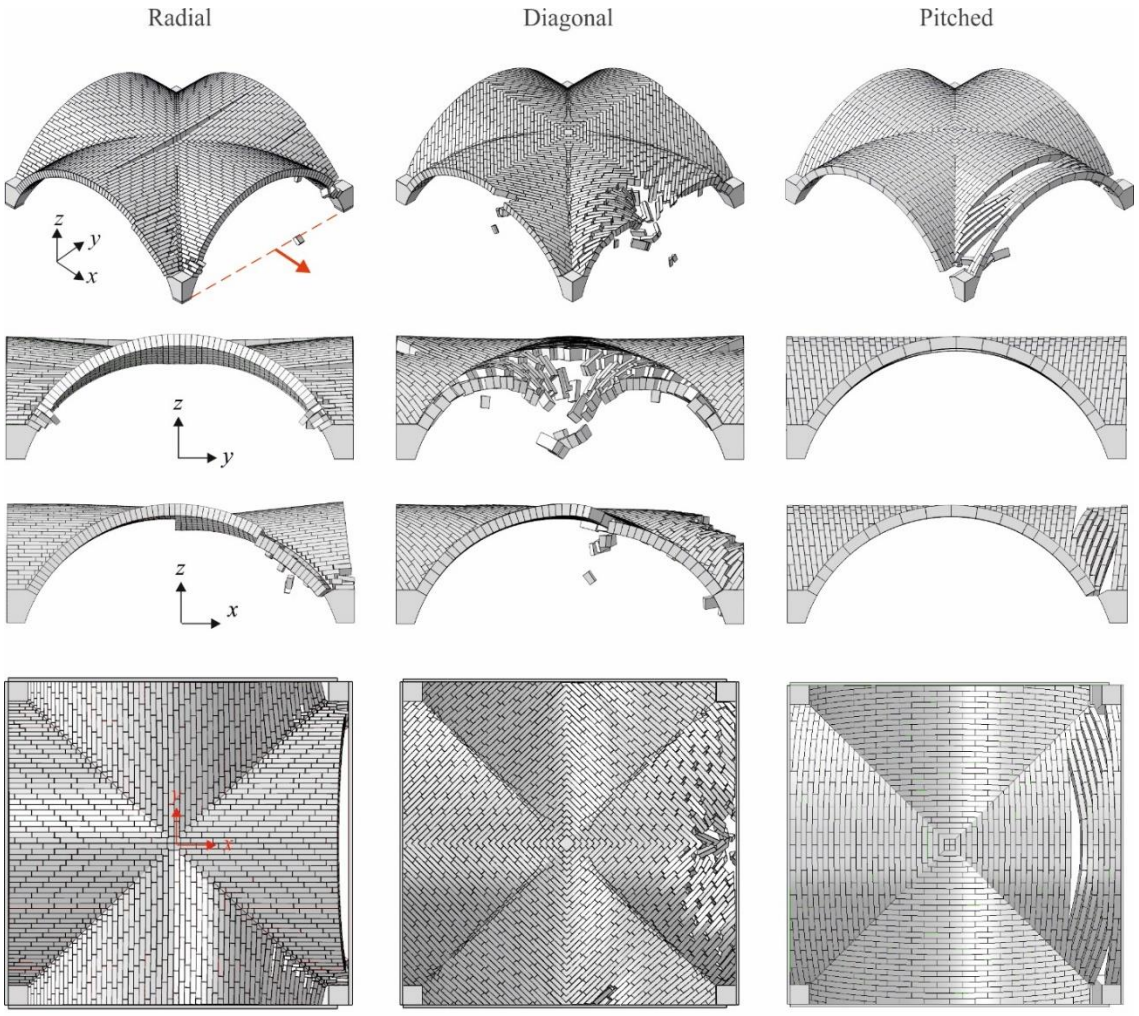

Figure 11: Deformed shapes for opening settlement: axonometric view (first row), y-z plane view (second row), x-z plane view (third row) and plan view (fourth row).

Figure 12 plots the isocontour of the vertical displacement u_z corresponding to the same opening settlement u_x/L= 3.3% (i.e., the maximum displacement reached by the diagonal vault) for all the brick patterns. The radial pattern shows a maximum value at the crown along the *y* axis, in correspondence of the hinge formation at the intrados. The vault with diagonal pattern has similar displacements in terms of magnitude, but very different distribution across the vault: higher vertical displacements are concentrated in the cap next to the moving abutments. The pitched vault remains almost undeformed and is characterized by a local failure of the cap next to the moving abutment that progressively involves brick courses towards the center of the vault.

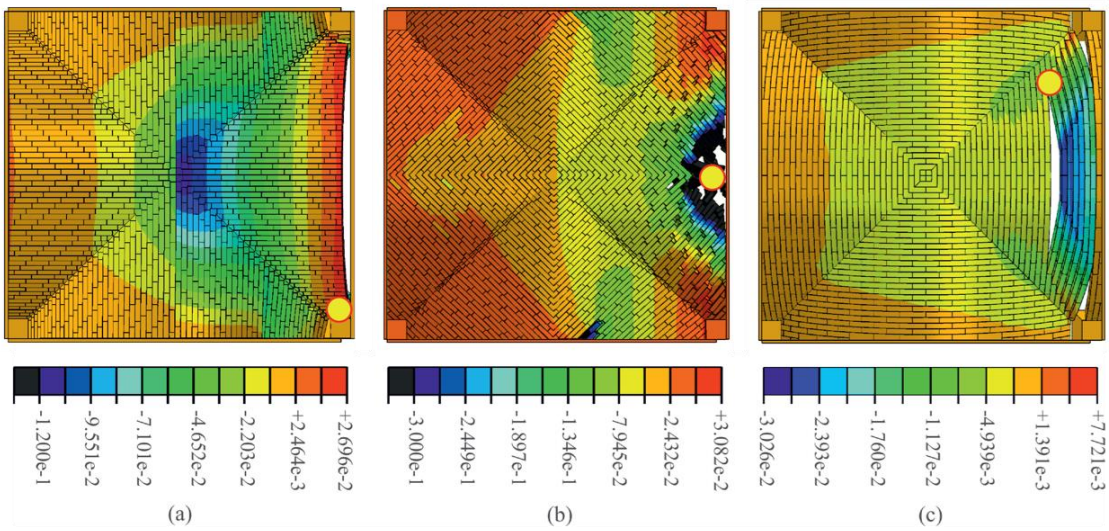

Figure 12: contour plot of u_z displacement [m] corresponding to an imposed opening settlement u_x/L= 3.3% for radial (a), diagonal (b) and pitched (c) pattern. Yellow circles refer to the monitored control nodes.

A deeper insight on the effects of brick pattern on the structural behaviour is provided through the load-displacement curves in Figure 13 toFigure 15. The curves are built by plotting the reaction force R in the direction of the applied displacement, scaled to the weight of the vault (W), versus the horizontal displacement of the moving support u_x divided by the span of the vault L. In particular, Figure 13a-b plot the horizontal thrusts at the abutments on the moving side of the vault ($R_{x,abt}$) and the resultants of the horizontal thrusts on the moving confining structure ($R_{x,con}$), respectively. The markers introduced in the mentioned Figures identify the displacement corresponding to the activation of a failure mechanism. Since such a mechanism may be either local or global, its occurrence may be not directly identifiable on the global force-displacement curve. For this reason, it has been determined by monitoring the differential vertical displacement Δu_z of the first two adjacent blocks which experience detachment and drop (Figure 14) and whose position is approximately highlighted by yellow circles in Figure 12: a sudden increase of such differential displacement corresponds to the activation of the mechanism. In general, Figure 13 toFigure 15 evidence a decreasing displacement capacity passing from pitched to diagonal to radial pattern. In particular, the pitched vault has the largest displacement capacity (twice the one of the diagonal one). It is worth noting that the horizontal thrust against the moving rigid boundary (Figure 13b) drop down to zero for very small horizontal displacements of the radial and pitched vaults. This means that the horizontal displacement, in these vaults, induces the head arches normal to the applied settlement to detach from the confining walls. In the diagonal pattern, where the diagonal brick courses are semi-arches that lie against the boundary structure on one side and against the groin on the other side, the vault continues to push on the rigid boundary until collapse and no detachment occurs. This can also be observed in Figure 11. In Figure 13c, the reaction force in x-direction along the two lateral fixed boundaries (on the x-z plane) shows that the latter are the structural elements which most contribute to the equilibrium of the vault.

Finally, Figure 13d reports the sum of the reaction forces discussed above. Observing the slope of the curves, it can be noted that the diagonal vault exhibits a greater increment of horizontal thrust with respect to the other two brick patterns for the same increment of imposed displacement.

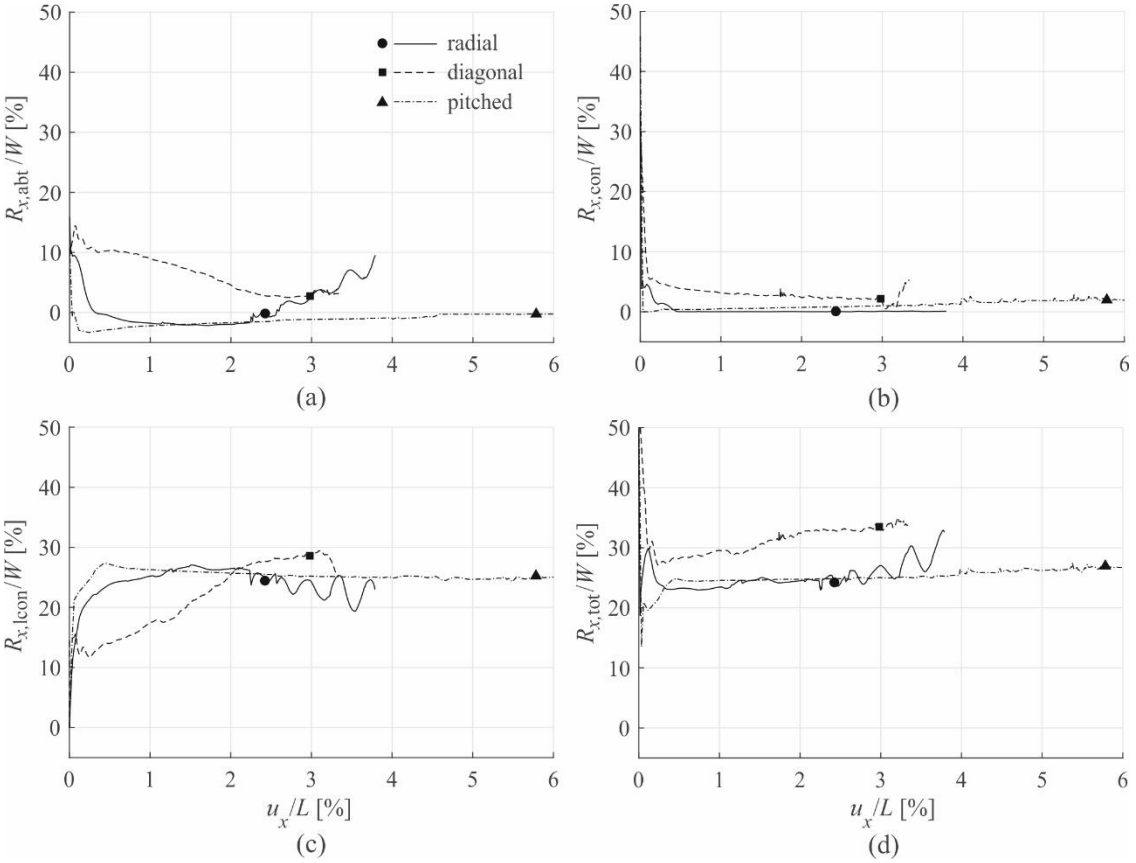

Figure 13: Reaction forces R_{x_abt} at the moving abutments (a), $R_{x,con}$ against moving rigid boundary (b), $R_{x,lcon}$ along lateral rigid boundaries (c) and $R_{x,tot}$ total (d) versus normalized imposed displacement for opening settlement

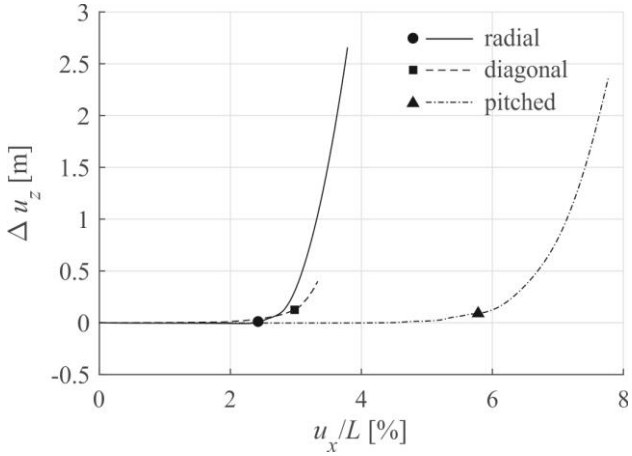

Figure 14: Differential vertical displacement versus normalized imposed displacement for opening settlement

Furthermore Figure 15 shows the vertical reaction forces R_z, highlighting the role of lateral rigid boundaries parallel to the direction of the imposed displacement. It can be noted that the pitched vault is the one that most relies on such boundaries, thanks to the friction induced by increasing normal compression forces between the lateral fixed constraints and the head arches of the vault. As a matter of fact, a sudden drop of R_z

at the abutments corresponds to an abrupt increase of the force at the lateral fixed boundary. This further clarifies the mechanism shown in Figure 11 for the pitched vault. Conversely, in the other two vaults the trend of R_z is almost constant at both the abutments and lateral constraints.

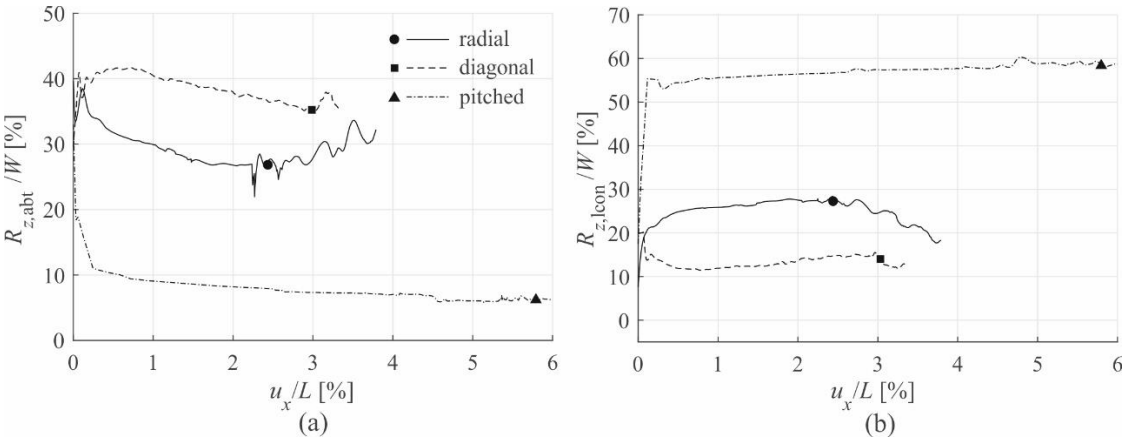

Figure 15: Reaction forces $R_{z,abt}$ at the moving abutments (a) and $R_{z,lcon}$ at the lateral rigid boundaries (b) versus normalized imposed displacement for opening settlement

It is noteworthy to observe that, if compared to the state of the vault with diagonal and radial pattern, the numerical analysis of the case with pitched pattern shows a very limited damage on the overall stability of the structure, proving that such orientation of the brick courses is more effective in preventing the structural collapse after a horizontal settlement at the abutments, in the presence of rigid lateral confinement.

4.2.2. Vertical settlement (V)

The results of vertical settlements of two abutments in RC vaults are analyzed, with the aim of simulating the effects of vertical foundation movement on a cross vaulted chamber confined by adjacent bearing structures.

The collapse mechanisms of each vault are depicted in Figure 16 and involve local failure whichever the brick pattern, even if according to quite different mechanisms. In the radial vault two cracks in *y* direction cause failure of the angular portion of the caps normal to the moving one. The vault with diagonal courses is subjected to a damage mainly localized in the proximity of the keystones belonging to the *x*-*z* planes and the global stability of the structure is ensured until high values of vertical displacements of the two adjacent abutments. In the pitched vault the local failure involves the detachment between the first three courses of bricks parallel to the ring arch connected to the moving abutments. These mechanisms can also be observed by looking at the contour plot of vertical displacements u_z (Figure 17) corresponding to the maximum settlement u_z/L = 1.47 % numerically reached by the pitched vault.

Figure 18 plots the different contributions to the normalized total vertical reaction forces (d) provided by the moving abutments (a), the moving boundary (b) and the lateral (*x*-*z* plane) fixed boundaries (c), respectively, versus the normalized imposed settlement u_z/L for the three brick patterns.

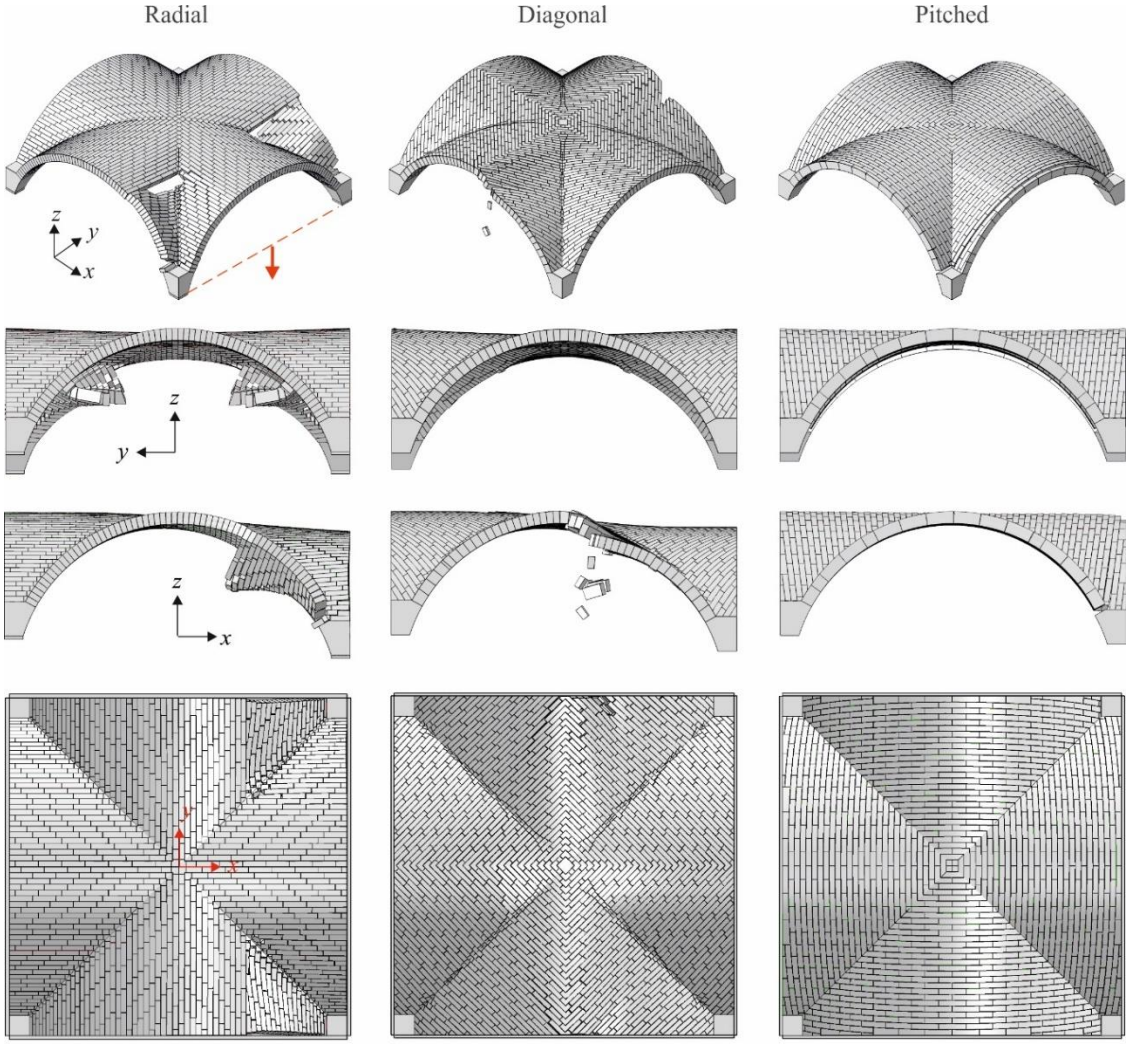

Figure 16: Deformed shapes for vertical settlement: axonometric view (first row), y-z plane view (second row), x-z plane view (third row) and plan view (fourth row).

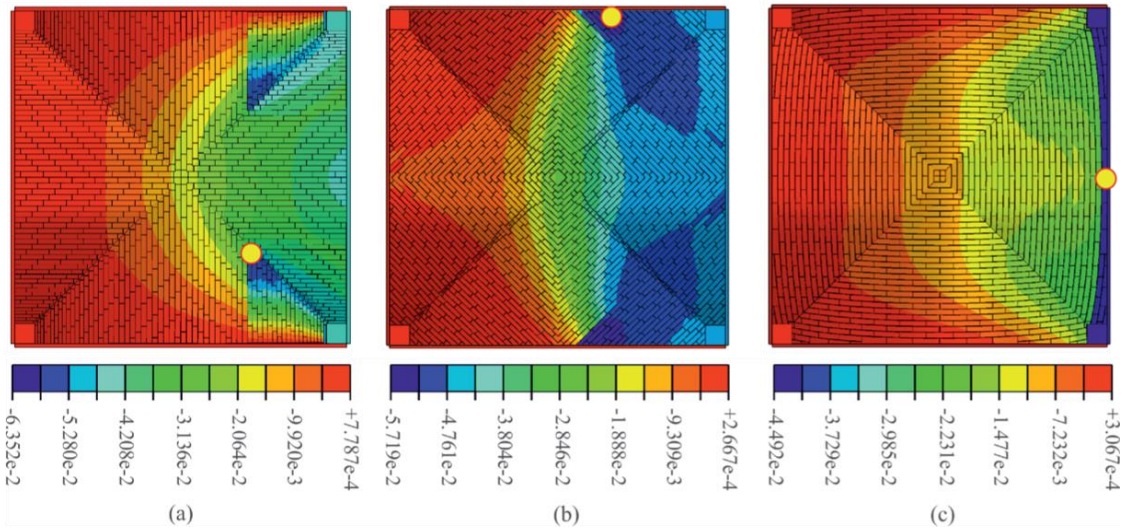

Figure 17: contour plot of u_z displacement [m] corresponding to an imposed vertical settlement u_z/L = 1.47 % for radial (a), diagonal (b) and pitched (c) pattern. Yellow circles refer to the monitored control nodes.

In all Figures, markers denoting the displacement capacity are identified according to the relative displacements of the control nodes (Figure 19) highlighted by yellow circles in Figure 17, showing that the local failure starts for increasing value of imposed vertical settlement from pitched to radial to diagonal vault. Despite some numerical instabilities characterize the curves, some considerations can be outlined by looking at their general trend. In the diagonal vault, the three contributions to the overall vertical reaction force are comparable and their trend is almost constant for increasing values of vertical settlement. This is due to the fact that this pattern assures the contact between the vault caps, rigid boundaries and abutments for every value of imposed settlement (Figure 16b). Conversely, in both pitched and radial vaults a detachment between the moving boundary and the adjacent cap causes the reaction forces at the moving boundary to drop assuming negative values. More specifically, in the pitched vault, the first brick courses slide and move downwards following the abutments and the moving boundary, while the remaining part of the vault remains stable thanks to the friction between the vault caps and lateral boundaries (Figure 16c): this behaviour is reflected in the load-displacement curves where, for increasing value of vertical settlement, the contribution of abutments and moving boundary decreases while the one of lateral rigid boundaries increases. Conversely, in the radial vault, the moving cap and the groins remain in contact with the abutments (Figure 16a), so that the reaction force at the abutments has a significant contribution to the overall vertical reaction force and the lateral rigid boundaries are less involved than in the pitched vault.

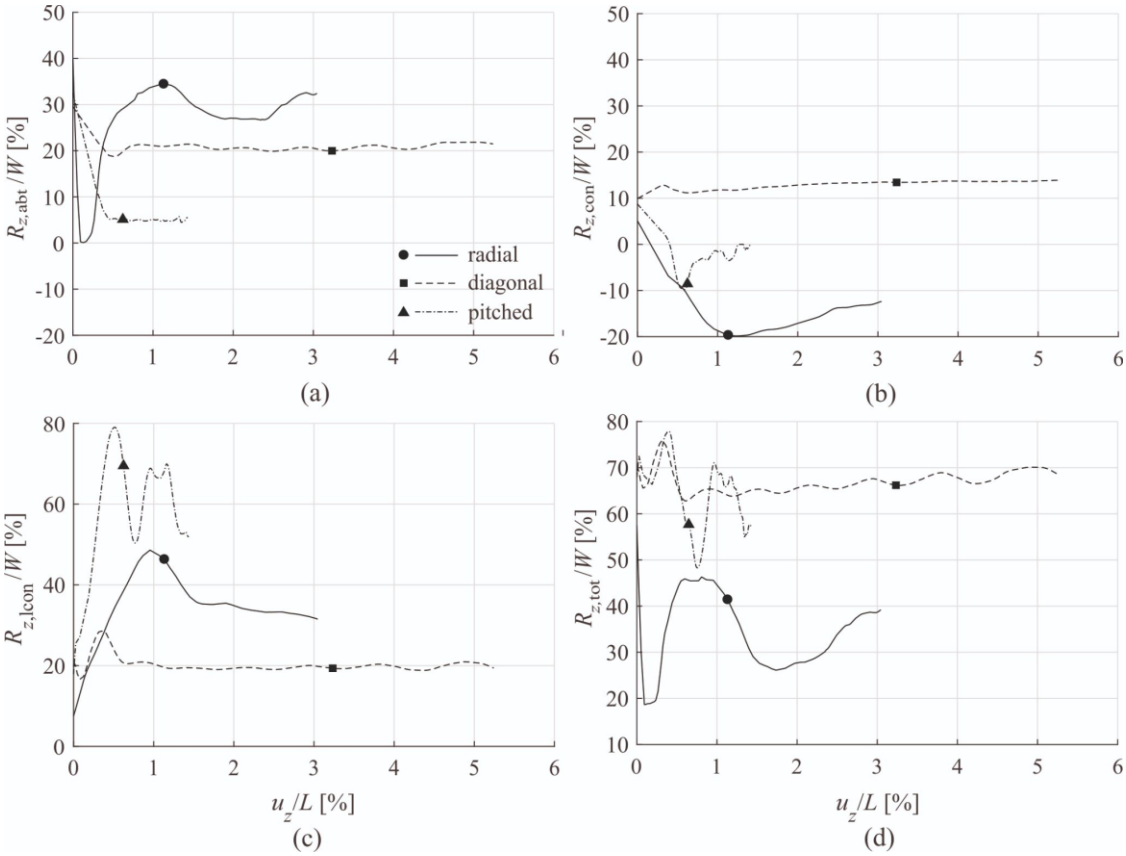

Figure 18: Vertical reaction forces $R_{z,abt}$ at the moving abutments (a), $R_{z,con}$ against moving boundary (b), $R_{z,lcon}$ along lateral rigid boundaries (c) and total reaction force $R_{z,tot}$ (d) versus normalized imposed displacement for vertical settlement

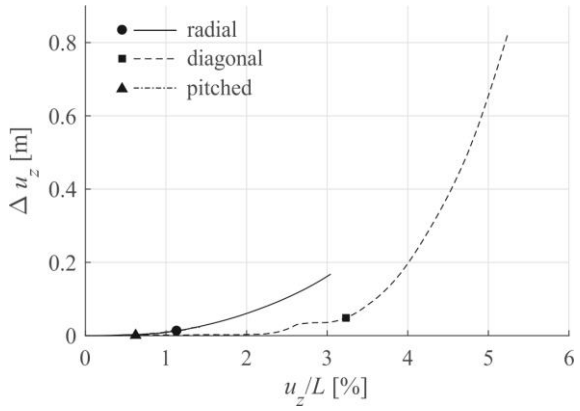

Figure 19: Differential vertical displacement versus normalized imposed displacement for vertical settlement

4.2.3.Shear settlement (S)

The influence of the brick pattern in vaulted structures under shear settlements is finally investigated for vaults endowed with lateral deformable arches.

The deformed shapes in Figure 20 testify the influence of the masonry pattern on the shear collapse mechanism. Note that, for a better reading of the Figures, deformed shapes are plotted without boundary arches, with the exception of plan views. In the radial vault, the collapse mechanism involves the formation of hinges parallel to the *y* axis and the formation of cracks along the shortened groin. When bricks are laid diagonally, a local failure starts from the moving corner due to formation of cracks along the diagonal courses. In the pitched vault, cracks develop along the courses near the abutments at the corner of the elongated groin. The different deformation mechanism induced by different brick laying is also highlighted by the distribution of vertical displacement u_z for fixed shear settlement u_y/L of 1.2%, which corresponds to the maximum displacement achieved by the pitched vault (Figure 21). The vertical sliding of parallel arches in the pitched vault induces vertical displacements one order of magnitude higher than those occurring in the other two types of vault.

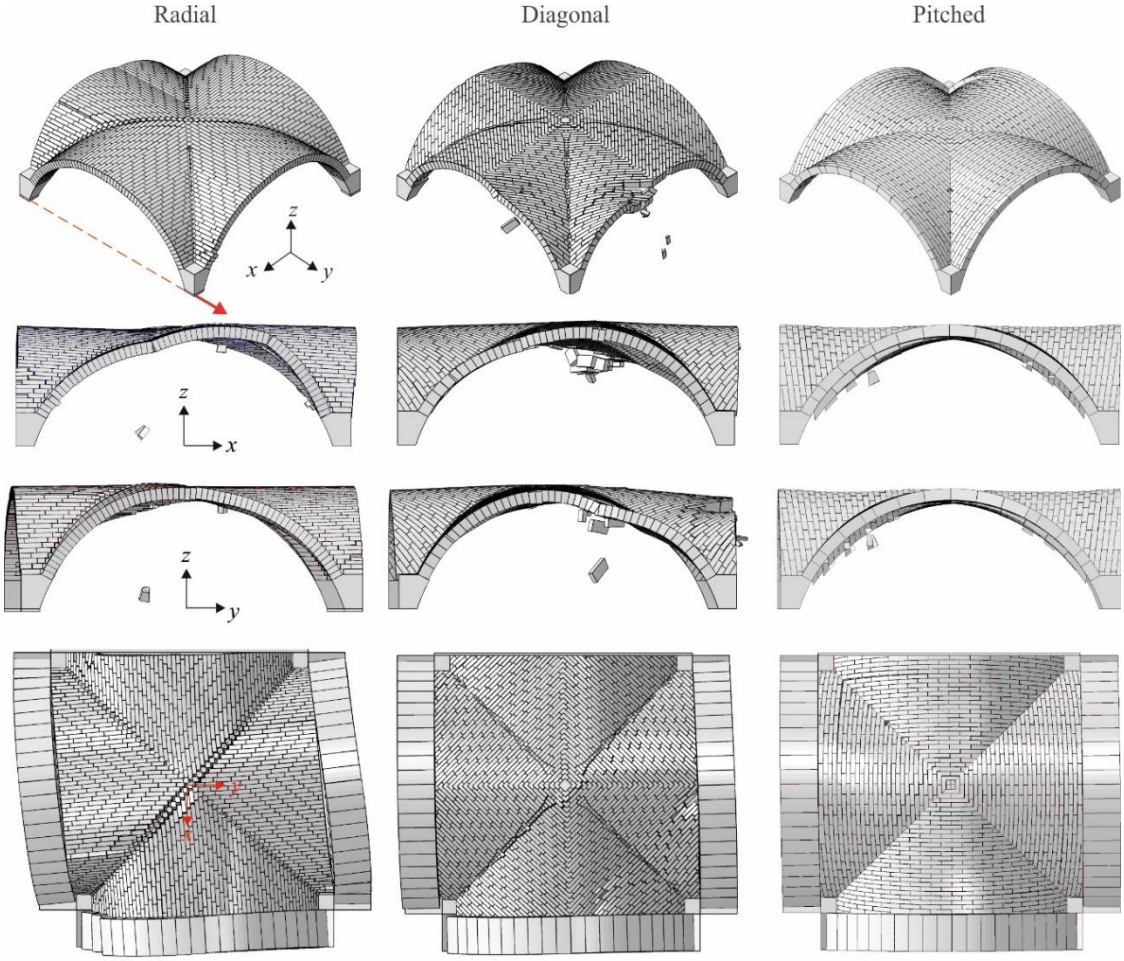

Figure 20: Deformed shapes for shear settlement: axonometric view (first row), y-z plane view (second row), x-z plane view (third row) and plan view (fourth row).

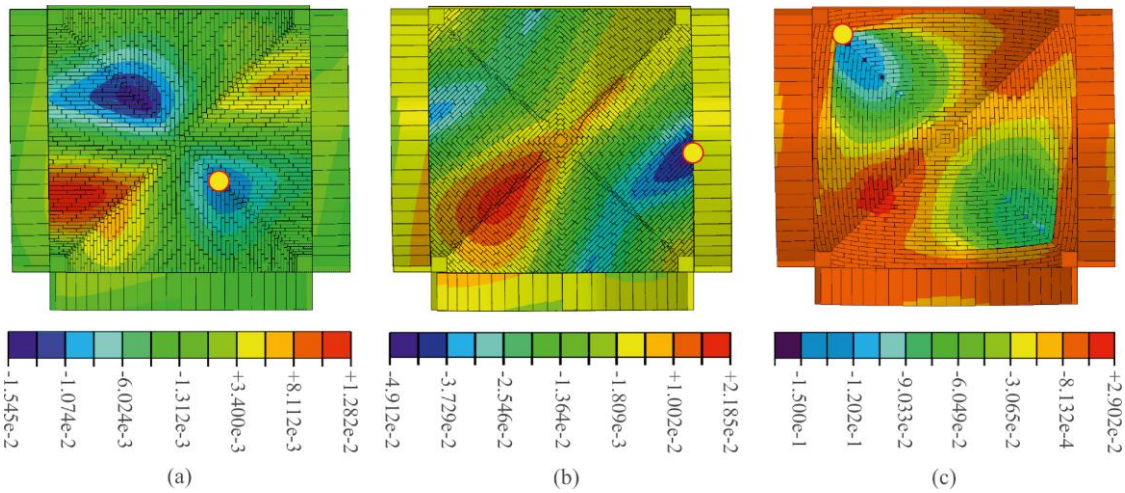

Figure 21: contour plot of u_z displacement [m] corresponding to an imposed shear settlement u_y/L = 1.2% for radial (a), diagonal (b) and pitched (c) pattern. Yellow circles refer to the monitored control nodes.

Figure 22 plots the resultant reaction forces at the vault moving abutments ($R_{y,abt}$ - Figure 22a) and on the confining structures ($R_{y,con}$ - Figure 22b), i.e., on the abutments of the deformable arches, in the direction of the imposed displacement versus u_y, while the total reaction force $R_{y,tot}$ is plotted in Figure 23a. The reaction forces are normalized to the vault weight W (without considering the deformable arches), while u_y is scaled to

the vault span L. Figure 22 allows observing the different contribution given by deformable arches to the overall reaction force in y direction: in the radial vault R_y is absorbed quite completely by DA (being negative the reaction at the vault abutments), while in both pitched and diagonal vaults the contribution of DA and vault abutments are almost the same. This means that, in the case of radial pattern, the head arch of the vault and the constraining perimeter arch exhibit a weak frictional connection in the y-z shear plane where sliding between vault blocks and DA occurs. Conversely, the inclined indenting of bed joints in diagonal vault and the longitudinal bed joints of the pitched vault, allow a better connection between the masonry blocks of the vault and the arched constraining elements. The markers in Figure 23a are referred to the value of imposed displacement that corresponds to the activation of a failure mechanism in each vault. They have been identified following the same criterion adopted for the opening and vertical mechanism, namely by referring to the sudden increase in the differential vertical displacement of two bricks plotted in Figure 23b and highlighted in yellow in Figure 21. In opposition to what was observed for the opening settlement, the displacement corresponding to the activation of the failure mechanism increases from pitched to diagonal to radial pattern.

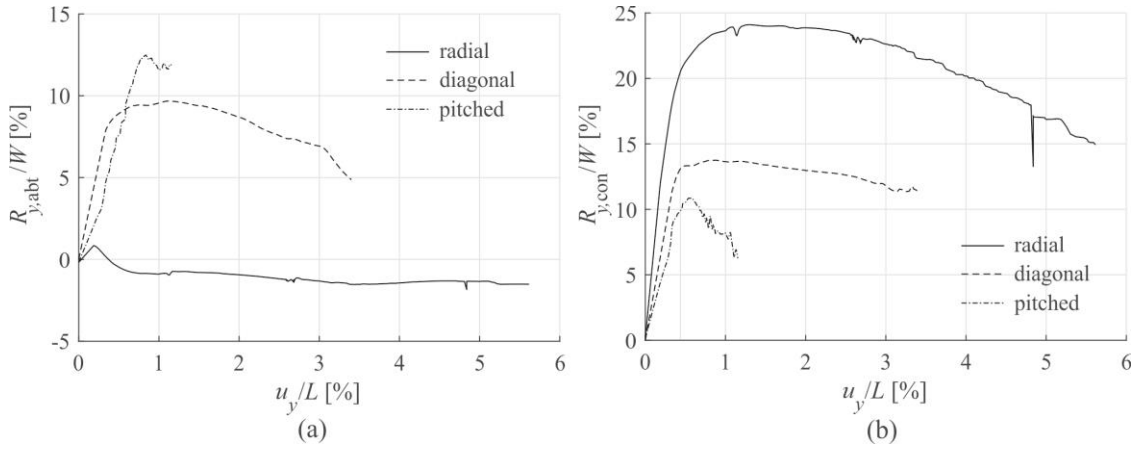

Figure 22: Reaction force $R_{y,abt}$ at the abutments of the vault (a) and $R_{y,con}$ of the deformable arches (b) versus normalized imposed displacement for shear displacement.

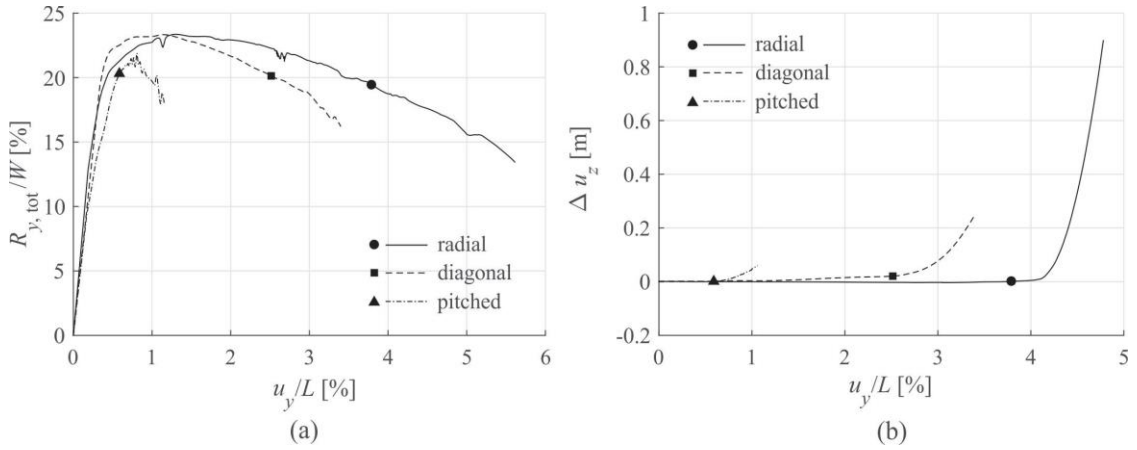

Figure 23: Total R_y reaction force versus imposed displacement (a) and differential vertical displacement versus normalized imposed displacement (b) for shear displacement.

In order to compare the load-displacement curves of total reaction forces (Figure 23a), the following quantities have been identified and reported in Table 5:

- R_{max}, peak value of the reaction force;
- u_c, imposed settlement corresponding to the activation of the collapse mechanism;
- K_{el}, elastic stiffness, calculated as the ratio R_{60}/u_{60} between the 60% of R_{max} (R_{60}) and the corresponding settlement (u_{60});
- u_{80}/u_{60}, ductility indicator, where u_{80} is the settlement corresponding to R_{80}, i.e., to a post-peak 20% reduction of R_{max} (note that u_{80} is assumed equal to the ultimate displacement u_{max} in case the reduction of R_{max} in the post-peak branch was less than 20%, e.g., in the pitched vault).

Moreover, Table 6 reports the variation of those terms with respect to the radial pattern case, as $\Delta Q = (Q_{pattern} - Q_{radial})/Q_{radial} * 100$, where Q is the generic quantity.

Table 5: values of critical quantities

Pattern	R_{max} [N]	u_c [m]	R_{60} [N]	u_{60} [m]	K_{el} [N/m]	u_{80} [m]	u_{80}/u_{60} [-]
Radial	6931	0.118	4159	0.0066	624974	0.125	18.82
Diagonal	7314	0.078	4389	0.0075	5819567	0.093	12.31
Pitched	6353	0.018	3812	0.0083	460956	0.036*	4.32

* $u_{80} = u_{max}$

Table 6: percentage variation of peak reaction force, elastic stiffness and ductility with respect to the radial configuration

Pattern	ΔR_{max} [%]	ΔK_{el} [%]	$\Delta(u_{80}/u_{60})$[%]
Diagonal	5.53	-6.88	-34.61
Pitched	-8.34	-26.24	-77.04

On the basis of the data reported in both Table 5 and Table 6, it can be observed that the three vaults have quite similar load capacity, with variations below 10% with respect to the radial pattern. Despite this, their behaviour is quite different in terms of elastic stiffness and ductility. Specifically, the pitched vault is the one characterized by the lowest elastic stiffness (26% lower than the radial vault) and the highest reduction of ductility with respect to the radial pattern.

4.3. Effects of boundary conditions and infill

The vault with radial brick pattern is used for investigating the effects due to the boundary conditions and the presence/absence of infilling material, for opening, vertical and shear settlements.

The qualitative collapse mechanisms of the vaults subjected to opening settlements are depicted in Figure 24 for confined/not confined vaults with/without infill. The deformed shapes correspond to the end of the load-

displacement curves reported in Figure 26. In this case, quite different collapse mechanisms characterize confined and not confined vaults. The confined vault is characterized by an asymmetric collapse mechanism due to the presence of lateral rigid boundaries which prevents the formation of the key hinge in the caps normal to the imposed displacement. Instead, a vertical sliding occurs, mainly involving the half of the vault close to the moving supports as clearly visible also in Figure 25a. Conversely, the collapse of the not-confined vault is symmetric with a typical a typical mechanism evolving from a three-hinge configuration. The latter is clearly visible in the vault without infill.

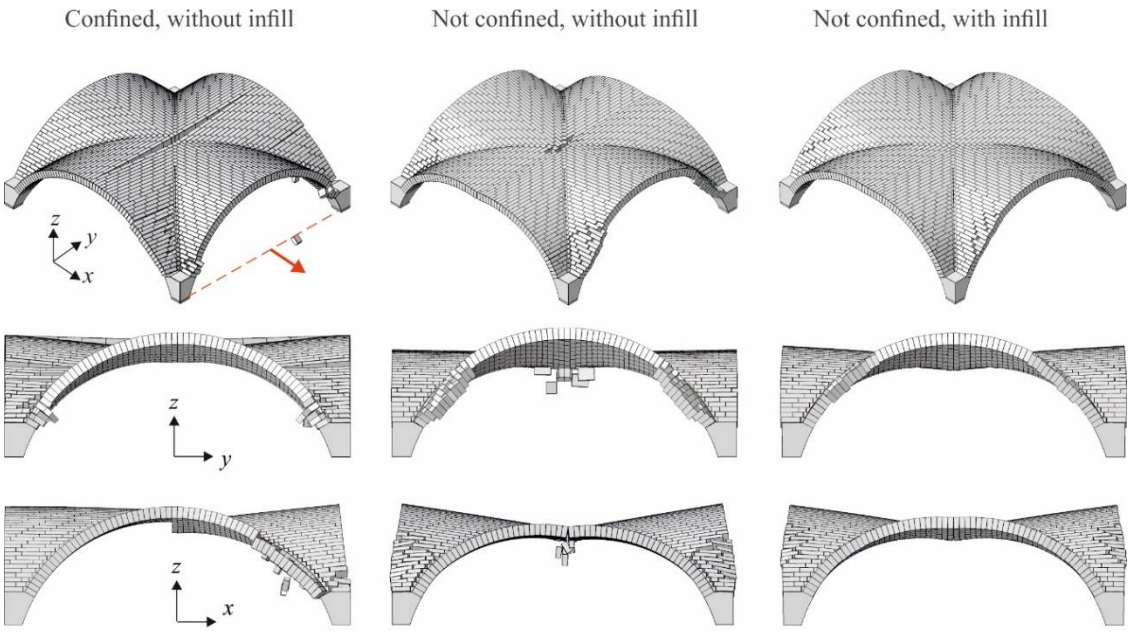

Figure 24: Deformed shapes for opening settlement: axonometric view (first row), y-z plane view (second row), x-z plane view (third row).

Figure 25 reports the comparison between vertical displacements corresponding to the same imposed opening settlement u_x/L= 3.3% and allows the effects of lateral confinement and infill to be further highlighted. Specifically, it can be observed that the presence of infill induces higher vertical displacement in the zone around the crown with respect to the case without infill.

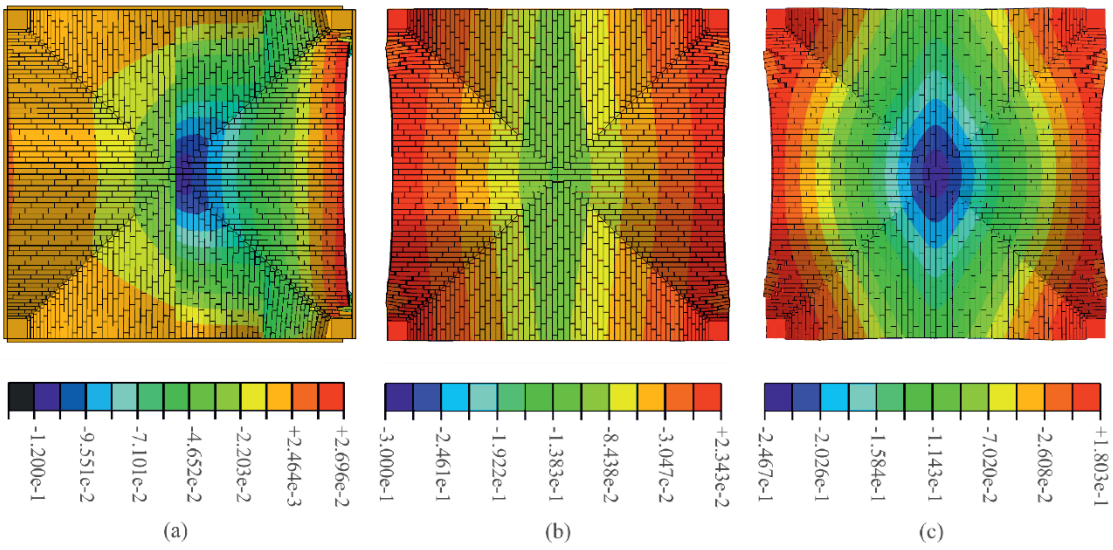

Figure 25: contour plot of u_z displacement [m] corresponding to an imposed opening settlement u_x/L= 3.3% for confined vault without infill (a), not confined vault without infill (b) and with infill (c)

The force-displacement curves are plotted in Figure 26 for the opening settlement. In particular, the total horizontal reaction force $R_{x,tot}$ is reported. In the case with infill, the reaction force is scaled with respect to the total weight of the vault, including the infill. It is worth noting that in the latter case the numerical analysis stopped before a clearly visible collapse mechanism due to converging issues. Nevertheless, the trend of the obtained curves allows some general observations to be outlined. In particular, in the presence of infill the slope of the curve is much higher than in the other two cases, meaning that for the same increment of imposed displacement, the increment of horizontal thrust ($R_{x,tot}$) of this vault is greater. On the other hand, the vault with infill is characterized by a reduced ductility. The NC and RC vaults exhibit a similar trend of variation of $R_{x,tot}$ for increasing values of imposed displacement.

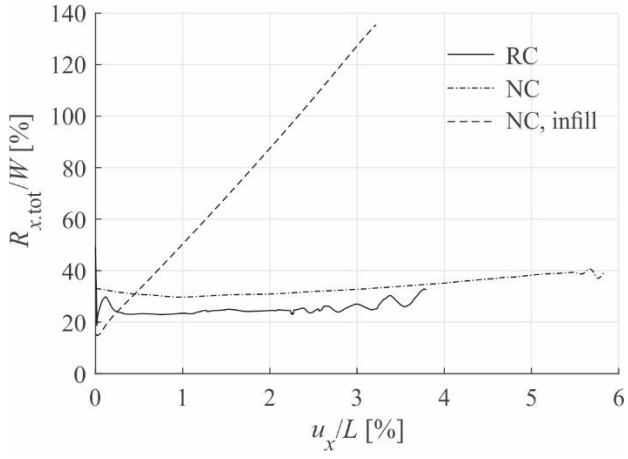

Figure 26: Comparison between total reaction force versus normalized imposed displacement in confined and not confined (NC) vaults, with and without infill, for opening settlement.

Similar observations than the ones discussed for opening settlement can be outlined also for the case of vertical settlement (Figure 27-Figure 28). The collapse mechanism is mainly influenced by the boundary

conditions (compare RC and NC vaults without infill), while the presence of infill in NC vaults does not significantly modify the collapse shape.

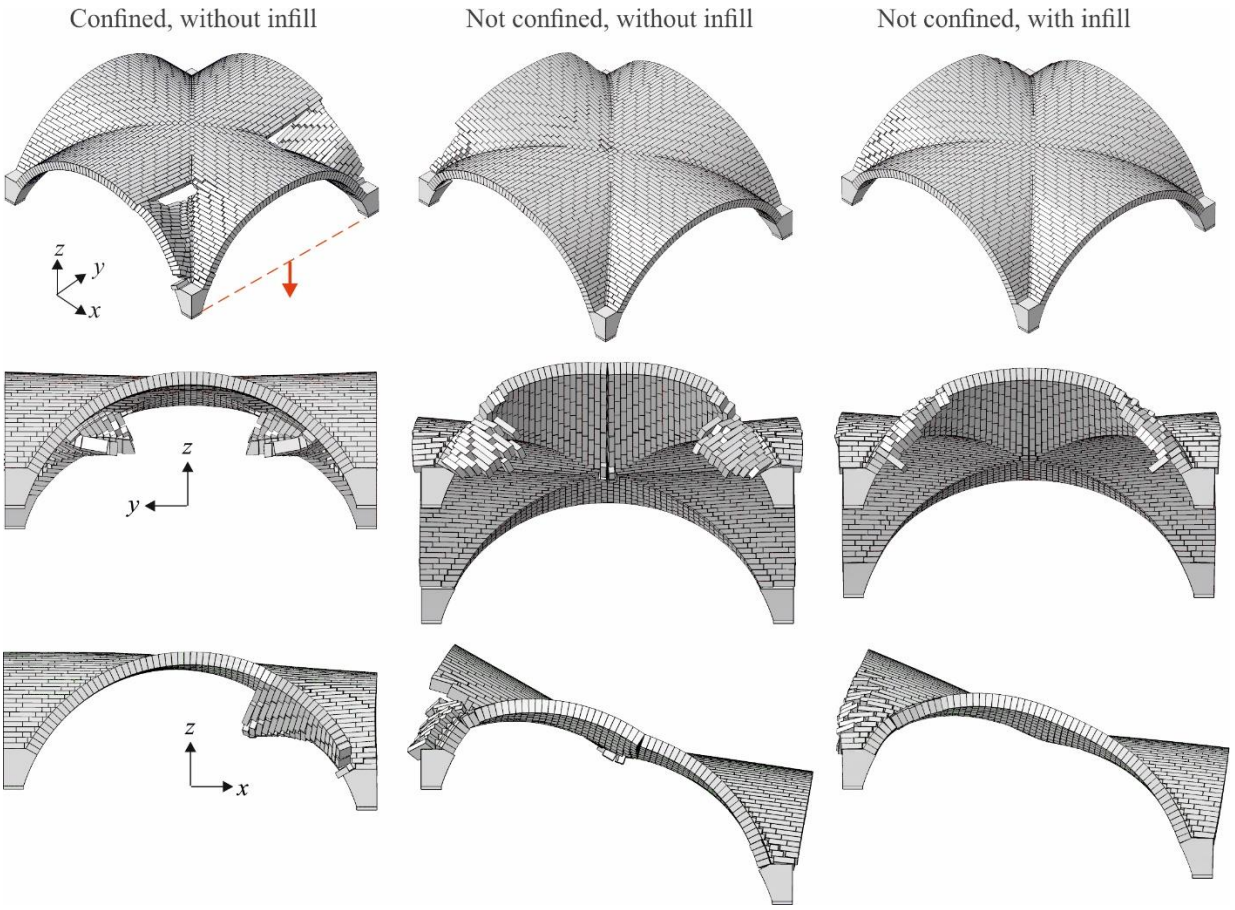

Figure 27: Collapse shapes for vertical settlement: axonometric view (first row), y-z plane view (second row), x-z plane view (third row).

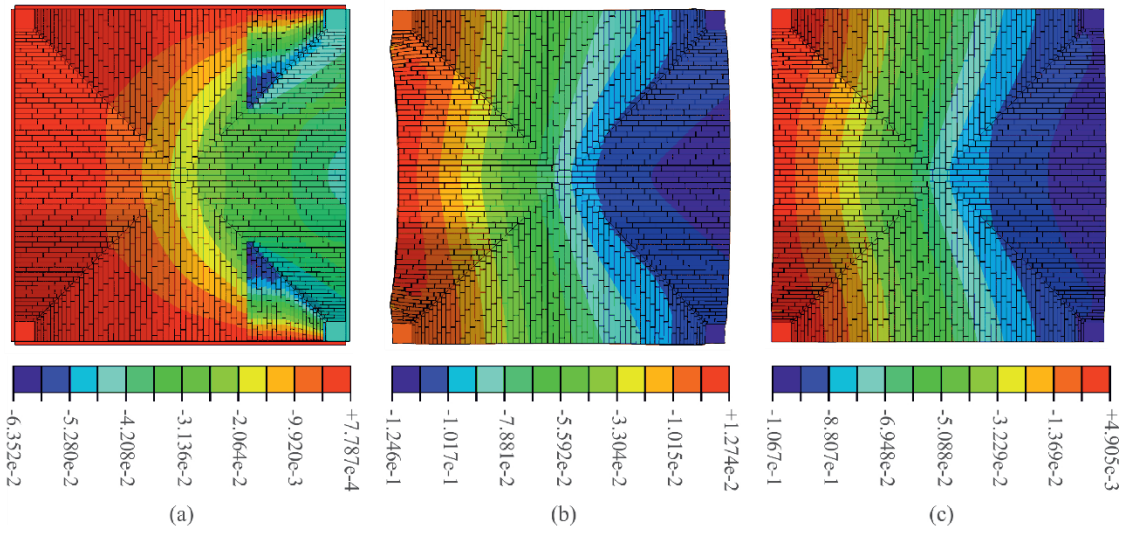

Figure 28: contour plot of u_z displacement [m] corresponding to an imposed vertical settlement u_z /L= 3.23% for confined vault without infill (a), not confined vault without infill (b) and with infill (c)

The vertical reaction forces versus imposed vertical settlement (Figure 29) show a similar trend as in the opening mechanism, i.e., NC and RC vaults display comparable capacity in terms of reaction force, while the presence of infill induces much higher increment of vertical reaction for the same increment of imposed displacement. As for displacement capacity, the NC vault without infill appears to be the one with the most ductile behaviour.

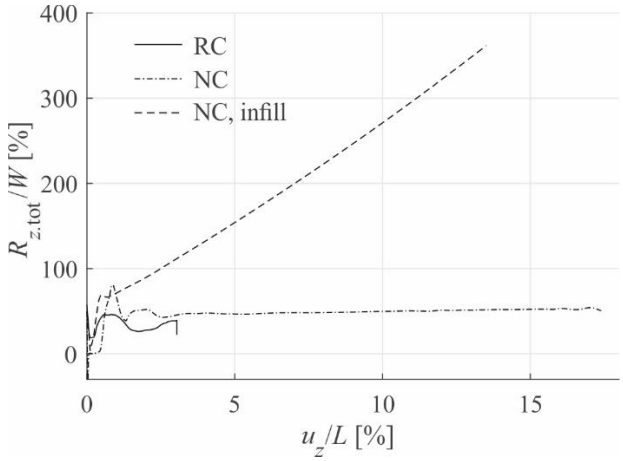

Figure 29: Comparison between reaction force versus normalized imposed displacement in confined and not confined (NC) vaults, with and without infill, for vertical settlement.

In the case of shear settlement, the influence of confinement and infill on the collapse mechanism is also evident (Figure 30), especially if looking at the contour plot of vertical displacements for the same imposed normalized shear settlement of 2.67%, which corresponds to the maximum achieved by the not confined vault with infill (Figure 31). First, it can be observed that the confined vault displays a non symmetrical deformation, due to the asymmetric boundary conditions (three deformable arches and one rigid boundary). Conversely, both not confined vaults have a symmetrical deformation where the diagonal groins are the axes of symmetry. Despite this general similarity, the distribution of vertical displacements is quite different depending on the presence of infill: in the vault without infill (Figure 30b), an extended portion of the vault around the shortened groin moves upwards; when infill is present (Figure 30c), upward displacement is limited to the four corners, while the rest of the vault moves downward.

The load-displacement curves depicted in Figure 32 are all characterized by an ascending branch until peak value of the reaction force is reached, followed by a descending branch. Both the vault where confinement is provided by deformable arches and the not confined vault display a similar behaviour, with a smooth decrease of the reaction force until high values of post-peak displacements. These two curves run almost parallel and differ for the higher bearing capacity due to the presence of the confinement. Conversely, the not confined vault with infill, which is characterized by the lowest elastic stiffness, reaches a higher capacity but has a shorter post-peak branch.

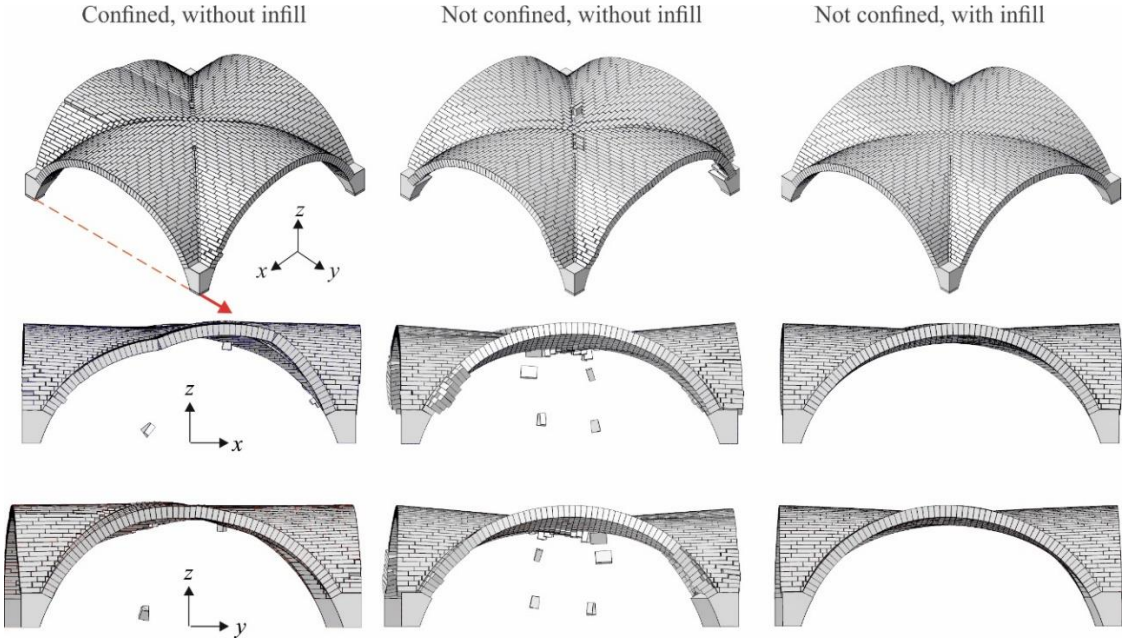

Figure 30: Collapse shapes for shear settlement: axonometric view (first row), y-z plane view (second row), x-z plane view (third row).

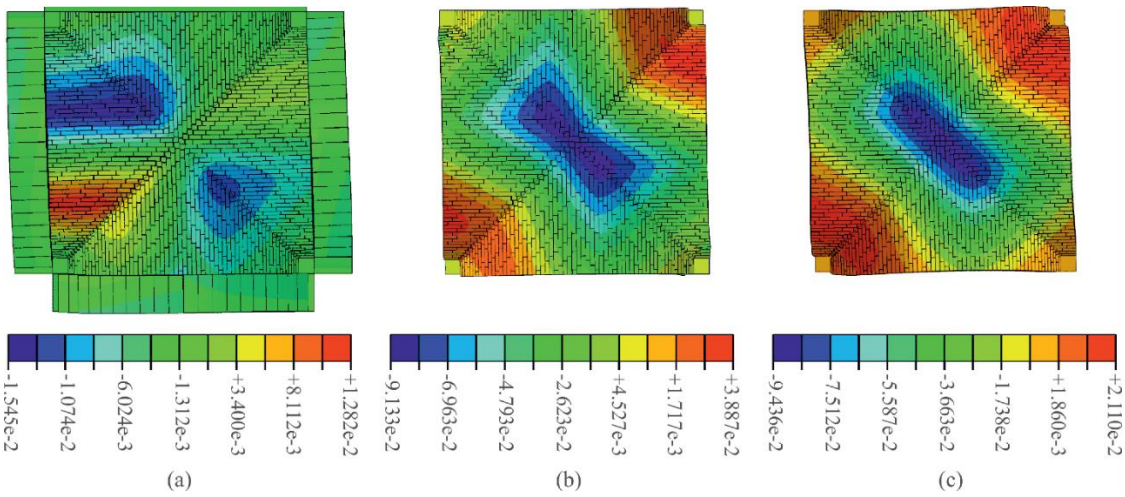

Figure 31: contour plot of u_z displacement [m] corresponding to an imposed shear settlement $u_y/L = 2.67$ % for confined vault without infill (a), not confined vault without infill (b) and with infill (c)

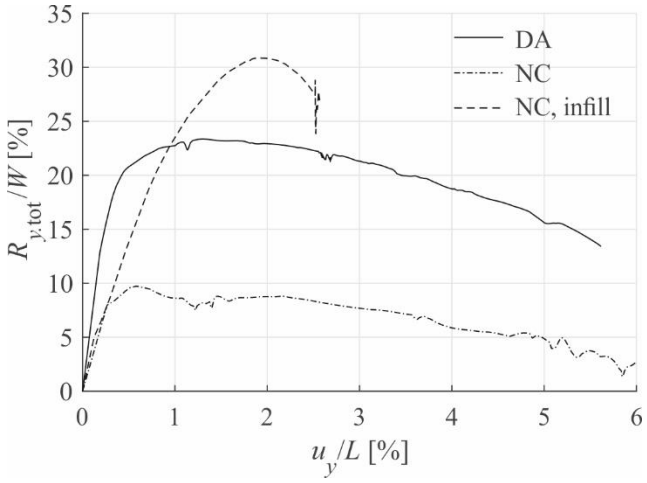

Figure 32: Comparison between reaction force versus normalized imposed displacement in confined (DA) and not confined (NC) vaults, with and without infill, for shear settlement.

It should be observed that in the vault with infill it was not possible to clearly identify a collapse mechanism as done in the other cases. For this reason, the amplified deformed shape at the intrados corresponding to the last analysis step is plotted in Figure 33, showing that several cracks are actually present and could be responsible for the activation of a possible collapse mechanism.

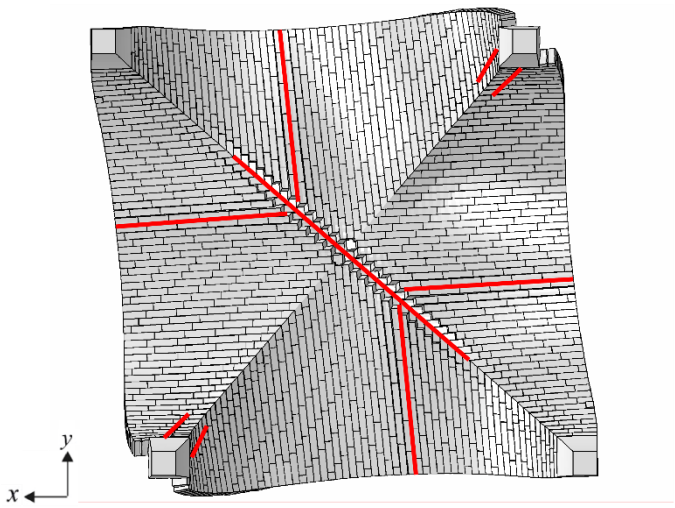

Figure 33: Crack pattern in not confined vault with infill (NC, infill), intrados view. Amplification factor: 6.

4.4. Crack patterns identification

On the basis of the results of the parametric analyses discussed in the previous sections, some typical crack patterns related to different masonry apparatus and boundary conditions can be outlined and summarized in the chart reported in Figure 34. This chart could help practitioners dealing with interventions on architectural heritage to properly interpret the possible reasons for a certain damage pattern on existing vaults. As a matter of fact, it is often difficult to identify the type of masonry apparatus, due to the presence of plasterwork or decorations at the intrados of the vault. Moreover, the identification of an undergoing settlement of the supports can be a challenging task.

By looking at the chart, it is possible to notice that the crack pattern changes quite drastically depending on the brick pattern of the vault, the boundary conditions and load cases. In particular, the patterns of cracks at the intrados and through thickness are of major interest for the practitioners, since in most cases the inspection of the extrados is not possible.

In the case of opening settlement (first row in Figure 34), the not-confined radial vault shows a typical symmetric three-hinges mechanism, with one crack visible at the intrados at the crown of the vault (blue line) and two cracks at the extrados (green lines) near the haunches. In the confined vaults, lateral rigid boundaries tend to localize the damage in the caps close to the moving abutments. In the radial vault they prevent the formation of the key hinge, determining instead a through-thickness crack (red line) produced by a vertical sliding. The confined diagonal and pitched vaults show local failures in the caps near the moving abutments. This is especially true for the pitched pattern, where different parallel cracks develop along the bed joints in the moving cap.

In the case of a vertical settlement (Figure 34 second row), when no confinement is provided the radial vault has intrados cracks visible at the key of all caps, with the exception of the one close to the moving abutments. When lateral boundaries are present, all the vaults develop cracks only on the side of the moving abutments. In the case of radial and diagonal vaults, such cracks are mainly located along the groins and the two caps along the y axis, while in the pitched vault they are located in the cap parallel to the x axis, adjacent to the moving abutments.

In the case of shear mechanism (Figure 34 third row) all the vaults show an almost antisymmetric crack pattern with the respect to the diagonals. The radial vault shows a similar crack pattern if boundary arches are present or not. Cracks develop along the bed joints, parallel to the directrix of each cap and a through-thickness crack is also visible on the shortened groin. When the vault is not provided with boundary arches, cracks are symmetric with respect to the groin's diagonal crack and are visible in all four caps; the diagonal crack is also flanked by several parallel ones, which are not visible in the confined vault. Conversely, when lateral confinement is present, through thickness cracks develop between the head arches and the boundary structures, except on the moving side. When bricks are laid diagonally, parallel cracks follow the direction of the bed joints normally to the elongated groin. In the pitched vault, cracks develop along the courses near the abutments at the corner of the elongated groin.

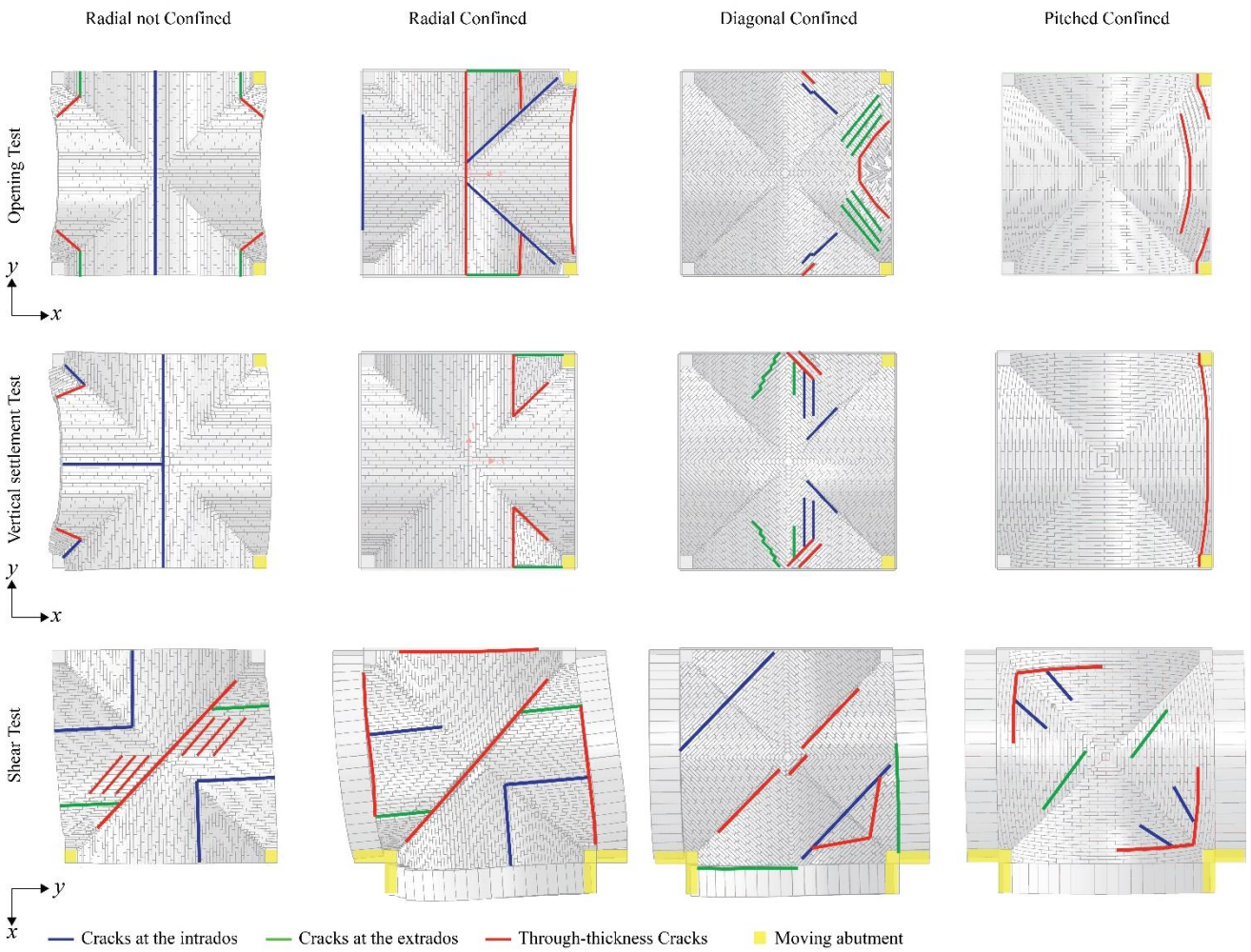

Figure 34: crack-pattern chart. Direction of moving abutments (in yellow): x-positive for Opening, z-negative for Vertical settlement, y-positive for Shear settlement.

5. Conclusions

In this paper the structural response of masonry cross vaults has been investigated using a contact-based finite element numerical approach. Simplified micro-modelling technique has been used for developing models of vaults with three different brick patterns, namely radial, diagonal and pitched. Parametric analyses have been performed for evaluating the difference in their structural response under a series of boundary and load conditions. In particular, three significant collapse mechanisms have been analysed, i.e., horizontal opening, shear sliding and vertical differential settlement of the vault abutments. The behavior of non-confined vaults has been compared with the response of structures endowed with either out-of-plane rigid lateral walls or perimeter deformable arches. Moreover, the effects of the presence of infilling material at the extrados have been investigated.

The results of the parametric analyses have shown that the masonry apparatus strongly influences the static behavior of masonry vaults in terms of collapse mechanism, bearing capacity and ductility. Moreover, the numerical analyses have demonstrated that it is not possible to identify a brick pattern which performs best in every load condition. The analyses have proved that the pitched vault exhibits the worst performances under shear and vertical settlements. Moreover, even though it proves to achieve the best performance against the opening mechanism, it has to be noted that such behavior is strictly related to the effectiveness of the restraining lateral walls to work as confining structures for the vault when the opening of the abutments occurs. These findings provide a probable explanation of the reason why this masonry pattern was rarely adopted in the construction history, at least in the European building tradition. The best performance of diagonal and radial vaults in vertical and shear settlement, respectively, depends on the different interlocking between blocks in the different directions. The diagonal vault is the one mostly interested by local collapses, whichever the imposed settlement.

As regards the influence of confinement and infill, the results showed that, when infill is present at the extrados of the radial vault, it provides lower displacement capacity to the structure, but increases the bearing capacity in the case of shear settlement. Moreover, the presence of rigid confinements is not always beneficial, causing the loss of contact between parts of the vault, thus resulting in local failures which reduce the displacement capacity.

The results of the parametric analyses allowed to generate useful crack-pattern charts for each masonry apparatus and for several boundary conditions, favoring the interpretation of the damage pattern on existing vaults. Such synoptic schemes aim at representing an efficient tool for architects and engineers involved in the path-to-knowledge and design of interventions on the Architectural Heritage of masonry constructions.

References

Abaqus Theory Manual, 2019, Dessault Systemes

Alforno, M., A. Monaco, F. Venuti and C. Calderini. 2020a. Validation of simplified micro-models for the static analysis of masonry arches and vaults, *International Journal of Architectural Heritage*, 1-17, DOI: 10.1080/15583058.2020.1808911

Alforno, M., F. Venuti and A. Monaco. 2020b. The structural effects of micro-geometry on masonry vaults, *Nexus Network Journal*, 22: 1237–1258

Baratta, A. and O. Corbi. 2012. The static behavior of historical vaults and cupolas. *Journal of Heritage Conservation*, 32: 65-81.

Barbieri, A., C. Carloni and A. Di Tommaso. 2004. Masonry orthotropic vaults in historical construction: the herring-bone pattern. In *Proceedings of the 4th International Conference on Arch Bridges ARCH 04* (Barcelona, Spain).

Boni, C., D. Ferretti and E. Lenticchia. 2021. Effects of Brick Pattern on the Static Behavior of Masonry Vaults, *International Journal of Architectural Heritage*, DOI: 10.1080/15583058.2021.1874565.

Breymann, G.A. 1849. Allgemeine Bau-Constructions-Lehre, mit besonderer Beziehung auf das Hochbauwesen. Vol. 1, *Constructionen in Stein*. Hoffmann, Stuttgart.

Calderini, C. and S. Lagomarsino. 2004. The effect of the masonry pattern on the global behaviour of vaults. In *Proceedings of the 4th International Conference on Structural Analysis of Historical Constructions* (Padova, Italy).

Chevalley, G. 1924. *Elementi di tecnica dell'architettura: Materiali da costruzione e grosse strutture*. Pasta, Torino.

Choisy, A. 1883. *L'art de batir chez les Byzantines*. Société anonyme de publications périodiques, Paris.

Curioni, G. 1870. *L'arte di Fabbricare. Costruzioni civili, stradali, idrauliche*. Negro, Torino.

D'Altri A.M, V. Sarhosis, G. Milani, J. Rots, S. Cattari, S. Lagomarsino, E. Sacco, A. Tralli, G. Castellazzi and S. de Miranda. 2019. Modeling strategies for the computational analysis of unreinforced masonry structures: Review and Classification. *Archives of Computational Methods in Engineering*, 27: 1153–1185.

Donghi, D. 1906. *Manuale dell'Architetto*. *Compilato sulla traccia del Bakunde des Architekten*. Utet, Torino.

Foraboschi, P. 2014. Resisting system and failure modes of masonry domes, *Engineering Failure Analysis*, 44: 315-337.

Formenti, C. 1893. *La pratica del fabbricare per l'ingegnere*. Hoepli, Milano.

Foti, D., V. Vacca, and I. Facchini. 2018. DEM modeling and experimental analysis of the static behavior of a dry-joints masonry cross vaults. *Construction and Building Materials*, 170:111–20.

Gaetani, A., N. Bianchini and P. Lourenco 2020. Simplified micro-modelling of masonry cross vaults: stereotomy and interface issues, *International Journal of Masonry Research and Innovation*, 6 (1): 97-125

Gelati, C. 1907. *Nozioni pratiche ed artistiche di architettura*. 2nd ed. (1st edition, 1899). Pasta, Torino.

Gelfi, P. 2002. Role of Horizontal Backfill Passive Pressure on the Stability of Masonry Vaults, *Internationale Zeitschrift für Bauinstandsetzen und Baudenkmalpflege*, 8(6): 573-590.

Ger Y Lobez, F. 1869. *Manual de Construccion Civil*. Imprenta de José Santamaria, Badajoz.

Huerta Fernández, S. 2001. Mechanics of masonry vaults: The equilibrium approach. In *Historical constructions. Possibilities of numerical and experimental techniques*, ed. P. B. Lourenco, and P. Roca 47–69. Universidade do Minho, Guimaraes.

Lassaulx, J.C. 1829. Beschreibung des Verfahrens bei Anfertigung leichter Gewolbeuber Kirchen und ahnlichen Raumen. *Journal fur die Baukunst*, 1(4): 317-330.

Levi, C. 1932. *Trattato teorico pratico di costruzioni civili, rurali, stradali ed idrauliche*. Hoepli, Milano.

Lourenço, P.B., J. G. Rots and J. Blaauwendraad. 1995. Two approaches for the analysis of masonry structures - micro and macro-modeling. *HERON*, 40 (4): 313-340.

Lourénço, B. P., R. De Borst, and J. G. Rots. 1997. A plane stress softening plasticity model for orthotropic materials. *International Journal for Numerical Methods in Engineering*, 40(21):4033–57.

Milani, G., P. B. Lourenço, and A. M. Tralli. 2006. Homogenised limit analysis of masonry walls, Part I: Failure surfaces. *Computers & Structures*, 95(7):541–61.

Milani, G., M. Rossi, C. Calderini and S. Lagomarsino. 2016. Tilting plane tests on a small-scale masonry cross vault: Experimental results and numerical simulations through a heterogeneous approach. *Engineering Structures*, 123: 300–312.

Romano, A., E. Grande. 2008. Masonry Barrel Vaults: Influence Of The Pattern. *14th World Conference on Earthquake Engineering*, October 12-17, 2008, Beijing, China.

Rossi, M., C. Calderini and S. Lagomarsino. 2016. Experimental testing of the seismic in-plane displacement capacity of masonry cross vaults through a scale model. *Bulletin of Earthquake Engineering*, 14: 261-281

Tralli, A., C. Alessandri, and G. Milani. 2014. Computational methods for masonry vaults: A review of recent results. *The Open Civil Engineering Journal*, 8:272–87.

Van Beek, G.W. 1987. Arches and Vaults in the Ancient Near East. *Scientific American*, 257: 96–103.

Wendland, D. 2007. Traditional vault construction without formwork: masonry pattern and vault shape in the historical technical literature and in experimental studies. *International Journal of Architectural Heritage*, 1(4): 311-365